METHODS AND MATERIAL DEVELOPED BEYOND CONVENTIONAL NANOIMPRINT

A Dissertation

by

BINGQING LUO

Submitted to the Office of Graduate and Professional Studies of
Texas A&M University
in partial fulfillment of the requirements for the degree of

DOCTOR OF PHILOSOPHY

Chair of Committee,	Jun Zou
Committee Members,	Xing Cheng
	Arum Han
	Zheng D Cheng
Head of Department,	Miroslav Begovic

December 2016

Major Subject: Electrical Engineering

ABSTRACT

Nanoimprint lithography (NIL) has been regarded as one of the next-generation lithography techniques due to its ability to fabricate nanoscale structures with low cost and high throughput. Although both thermal and UV nanoimprint have demonstrated sub-10 nm resolution, the adoption of NIL by industry has been very limited. The main reasons are that the density of pattern defects and low throughput cannot satisfy the stringent requirement of commercial lithographic technique. In this study, methods and material have been developed to overcome the limitations beyond conventional nanoimprint by utilizing three main factors: mold, the interface between mold and resist, and resist.

In the study, we first developed a new synergistic thermal and UV nanoimprint lithography (STUV-NIL). A transparent mold is integrated with a transparent metal oxide heater, which enables resists to be cured by thermal energy and UV light spontaneously. This new STUV-NIL combines thermal and UV techniques into one module and helps throughput improvement and reducing mold-resist adhesion and hence defect generation.

In the second part of this study, the thermal behavior of a polycarbonate resist was investigated by characterization of polycarbonate gratings reflow after thermal annealing. The observation of exceptional thermal stability of entangled polycarbonate polymer opens up new routes of step-and-repeat thermal nanoimprint and high resolution patterning.

The adhesion characteristic between polymers and the mold is a critical factor in the demolding process. In the third part of our study, polycarbonate residual layer has been applied as an anti-sticking treatment on nanoimprint molds, replacing the self-assembled monolayer currently used. It satisfies the requirements of not only low surface energy but also low reactivity for durability.

Polymerizations in UV NIL are generally accompanied by shrinkage in volume, which causes serious problems such as residual stress, demolding problems and defects. Epoxy-based UV resists have a volume shrinkage in the range of 3% to 10%. In the fourth part of our study, spiro-orthocarbonate, which undergoes volume expansion upon cationic ring-opening polymerization, has been mixed with an epoxy monomer to adjust the volume shrinkage of the cured resist and achieve zero volume change after curing.

DEDICATION

For my whole family and sweet boyfriend, Zhaojie Tong.

ACKNOWLEDGEMENTS

I would like to express my sincere thanks to my Ph.D. advisor, Dr. Xing Cheng, for his tremendous support and advice throughout my study at Texas A&M University and Southern University of Science and Technology in China. His consistent training, guidance, and encouragements have broadened my horizon of knowledge and taught me the spirit of doing research. Inspired by his enthusiasm and insight in the forefront scientific research, I also make myself being devoted to my academic and research work. I am very fortunate to have an enjoyable and rewarding research life in his group.

I am indebted to my thesis committee members, Dr. Jun Zou, Dr. Arum Han, and Dr. Zheng D Cheng, who spent their precious time serving on my advisory committee and offering suggestions on my research work and graduation schedule.

My sincere appreciation goes to my former and current group mates in Nano & Microelectronics Research Laboratory, including Dehu Cui, Youwei Jiang, Yulong Chen, Ziping Li, Bo Yu, Zengju Fan, Zhong Zhang. It is a pleasure to work with them, share experiences and discuss the scientific research. In particular, thanks Dehu for helping me in many ways, such as instructing me to use the semiconductor processing facilities, sharing my joys and frustrations, and much more.

I would also like to thank Dr. Yanqing Tian in Southern University of Science and Technology in China for providing valuable help in the chemical synthesis and analysis.

I am grateful to Young Thousand Talent research fund for supporting the work. The countless help from Mrs. Tammy Carda on the academic coordination related to my Ph.D. work is also highly appreciated.

My deep gratitude goes to my parents and brother for their continuous love and encouragement, and my boyfriend, Zhaojie, for always being there for me. Whenever life gets hard, I know that we still have each other.

CONTRIBUTORS AND FUNDING SOURCES

Contributors

This work was supervised by a dissertation committee consisting of Professor Xing Cheng [advisor], Professor Jun Zou and Professor Arum Han of the Department of Electrical Engineering and Professor Zheng D Cheng of the Department of Chemical Engineering.

All work for the dissertation was completed by the student, in collaboration with Southern University of Science and Technology in China.

Funding Sources

Graduate study was partially supported by a fellowship from Texas A&M University and this work was supported by Young Thousand Talent research fund of China.

TABLE OF CONTENTS

Page

LIST OF FIGURES

Page

LIST OF TABLES

Page

CHAPTER I

INTRODUCTION AND LITERATURE REVIEW

1.1 General Introduction

Since the first silicon-based metal oxide semiconductor field effect transistor (Si-MOSFET) was invented in the mid-60s, for past decades, shrinking the device feature size has been a driving force for the development of the semiconductor technology and integrated circuit (IC) industry. With decreasing the feature size, the device's performances can be greatly enhanced and at the same time, high degree of integration significantly lowers the cost of integrated circuit (IC) production. The conventional optical lithography has supported continuous reduction in device size required by the semiconductor IC industry. However, this shrinkage trend is blocked by the resolution limit of conventional lithography techniques, which is fundamentally related to the wavelength of the exposure light. In recent years, the requirement for sub-100 nm feature size devices has stimulated the lithography technique to new levels in semiconductor industry. Next generation lithography (NGL) tools have been proposed including immersion-assisted photolithography, 157-nanometer lithography, extreme ultraviolet (EUV) lithography, projection-electron lithography [1], electron beam lithography (EBL) [2], and X-ray proximity lithography [3]. However, all these technologies systems are very complicated and expensive, and various technical barriers need to be overcome before practical use for manufacturing. New lithographic

techniques are imperative needed for high resolution and low cost in micro- and nano-fabrication.

1.2 Next Generation Lithography

According to the International Technology Roadmap for Semiconductors (ITRS) report in 2015 (Figure 1): extreme ultraviolet lithography (EUVL), directed self-assembly (DSA) and nanoimprint lithography (NIL) are proposed as candidates for the next-generation (7 nm node and beyond) lithography techniques. However, EUVL [4-6] needs an expensive lens, lacks a suitable light source, and material absorption due to its high energy remains an issue; and directed self-assembly (DSA) [7, 8] has the defect issue. A high resolution and low cost lithography tool needs to be developed.

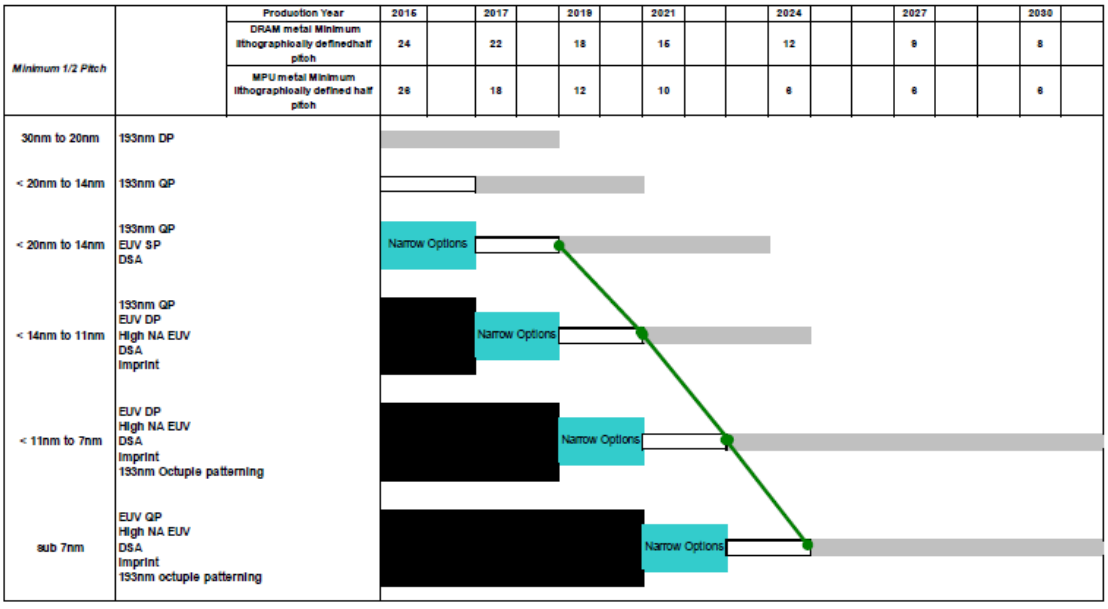

Figure 1 ITRS Report, 2015: http://www.itrs.net/.

1.3 Nanoimprint Lithography

Since 1995, nanoimprint lithography (NIL), initially demonstrated and developed by Stephen Chou's group [9, 10], has emerged as one of the most promising lithography tools for high-throughput, high resolution, low cost, and simple nanoscale patterning. It consists of transferring the pattern from a mold to a resist layer through application of elevated temperature and high pressure or UV light. Depending on which mechanism is used, NIL can be categorized into thermal NIL and ultraviolet NIL. The schematics of both NIL processes are shown in Figure 2. In both techniques, a mold is first fabricated by high resolution lithography such as EBL and reactive ion etching (RIE). Then the mold is treated with a surfactant coating for anti-sticking effect in the demolding process.

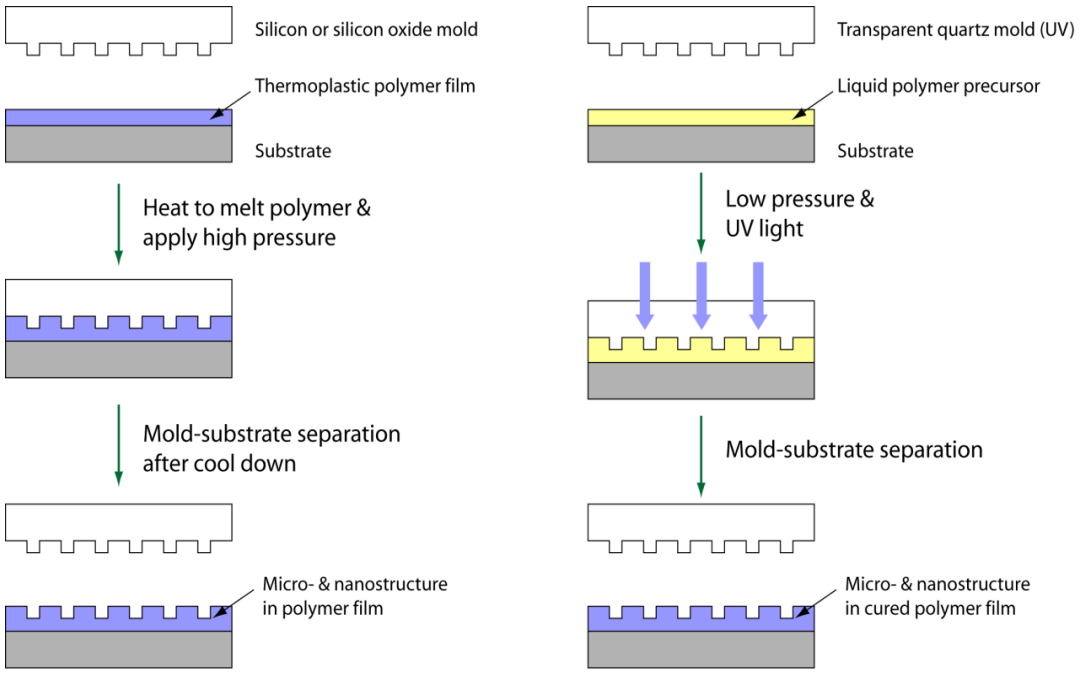

Figure 2 Schematics of thermal nanoimprint and UV nanoimprint lithography.

For thermal NIL, a thin layer of thermoplastic polymer is spin-coated on the substrate. The mold is brought into contact with the polymer-coated substrate and then the whole assembly is heated up to 70-80 ℃ above the polymer's glass transition temperature (T_g) and applied a suitable pressure, thereby imprinting contrast patterns in the polymer layer. After cooling down to the room temperature (RT), the mold is released from the substrate and the solidified patterns are formed on the substrate. At the same time, a thin layer of resist is often left underneath the patterns, which is referred as residual layer, and commonly needs to be removed by oxygen reactive ion etch for succeeding applications.

With simple tools and processing, thermal NIL has demonstrated sub 10 nm resolution [11], 3D patterning capability [12] and multi-level alignment with sub 500 nm accuracy [13]. Compared to traditional photolithography, this imprint process can easily scale down the feature size without limitation in resolution, and the minimum replication pattern is only limited by the mold pattern size. The thermal polymer resists (most conventionally poly(methyl methacrylate) (PMMA) or polycarbonate) and nanoimprint tools are commercially available at low price, which make thermal NIL a cost-efficient lithographic technology for mass production. The compatibility of patterning diverse polymers enables great potential in applications in the field of nano-electronics [14-20], nano-magnetic [21], and nano-biology [22-25].

For UV NIL, a UV curable liquid material is used as the alternative resist. The mold used in UV NIL must be highly transparent to UV light and is often made of fused silica. UV curable imprint resist is spin-coated on a substrate and pressed by the mold

with a low pressure. While maintained being pressed, the whole assembly is irradiated by UV for curing. Once the resist is cured and hardened, the mold is released.

UV-NIL utilizes UV induced polymerization to convert the imprinted liquid patterns to solid form, enabling the imprint pressed under a relative low pressure at room temperature, which are distinct advantages over its counterpart thermal NIL. The UV resist can be cured by UV irradiation within a few seconds while more than 10 min is necessary in thermal NIL for the heating up and cooling down stages. Hence UV NIL yields a higher throughput.

If the UV curable resist is dispensed on a substrate, the process would be called step and flash imprint lithography (S-FIL), which is first introduced by Grant Willson's group in 1999 [26]. The steps of S-FIL are shown in Figure 3. S-FIL is very attractive in modern microelectronic industry because of its easy step and repeat imprinting (Figure 4) [27] over large substrates, which leads to major applications in integrated circuit fabrications.

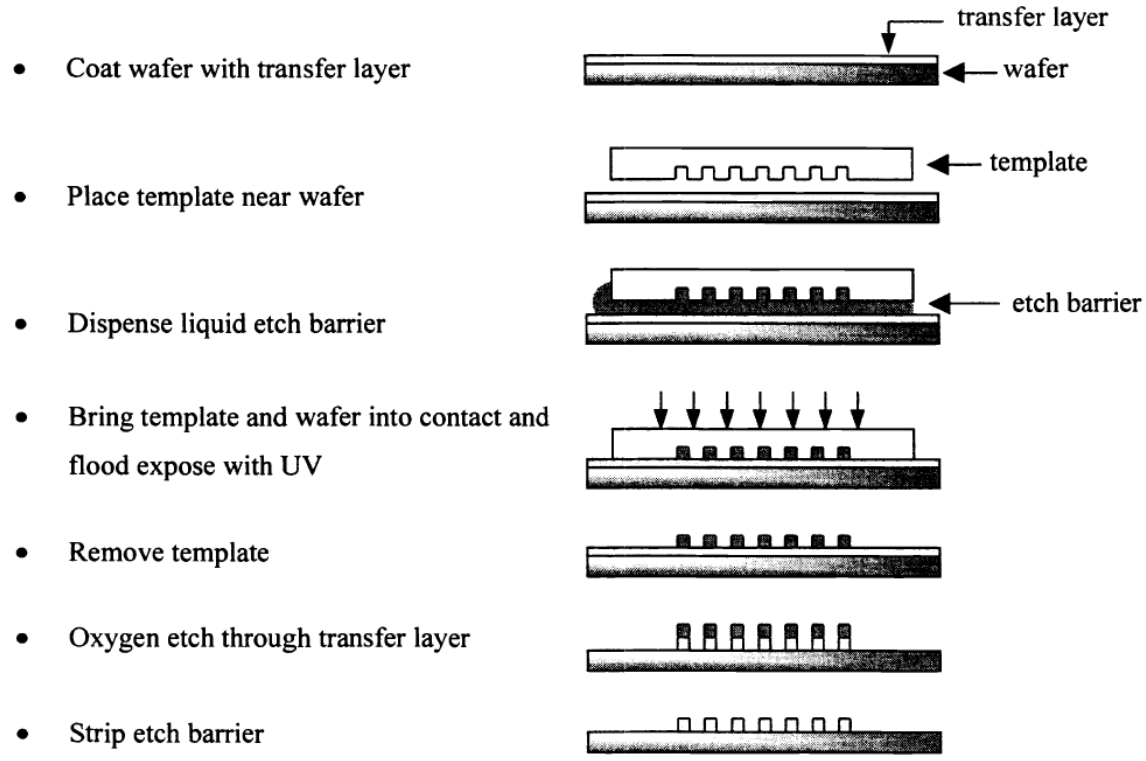

Figure 3 Schematics of the SFIL process [26].

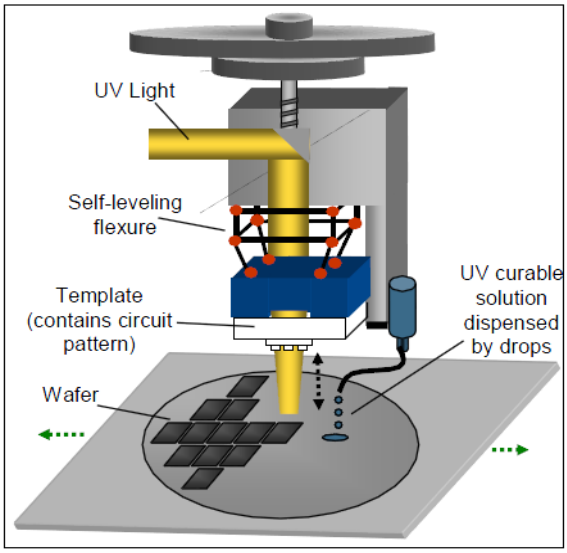

Figure 4 Schematics of the step and repeat NIL process [27].

1.3.1. Nanoimprint tools

Since NIL has attracted great attention and stimulated huge interest in academic research and industry, it promotes the development of business in nanoimprint tools and solutions. Since the invention of the nanoimprint technique, there are now at least 5 nanoimprint tool vendors, and more than 10 nanoimprint template and service providers. There are many corporations focusing on this business field, such as Nanonex, Molecular Imprints and etc. A manual hydraulic press machine (Specac Co.) applied in thermal NIL is shown in Figure 5. The machine mainly consists of two heating platens and a pressing tool, which can be conducted imprint with adjustable pressure and temperature for thermal NIL. A compact full-wafer imprintor (Nanonex NX-2500) is shown in Figure 6, enabling both thermal and UV NIL, and is able to achieve full wafer (up to 6") processing with sub-micron overlay alignment accuracy.

Currently a variety of novel nanoimprint tools is commercially available. The LithoFlexTM 350 (Molecular Imprints Co.) is configurable for plate-to-roll or roll-to-plate imprint, which leads to great flexibility and high throughput. The NX-2600 (Nanonex Co.) integrates NIL with photolithography technique, which can perform all forms of nanoimprint and high resolution photolithography. The development in NIL research has made this technology competitive with the mainstream next generation lithography techniques.

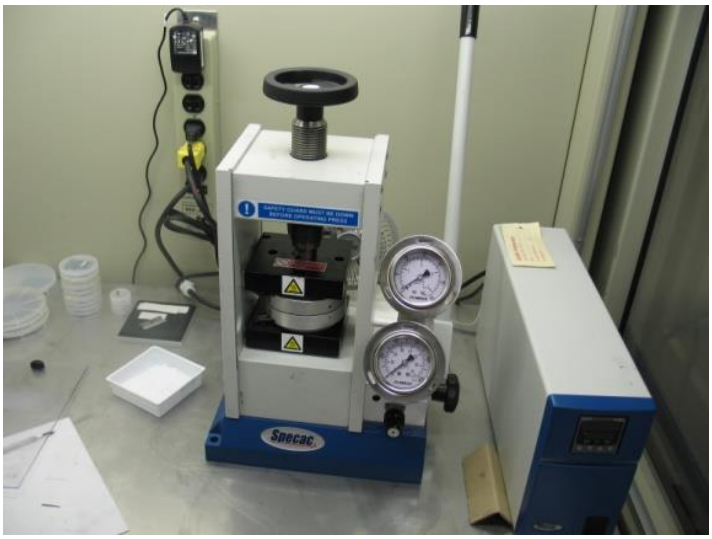

Figure 5 Hydraulic press machine.

Figure 6 Compact full-wafer imprintor.

1.3.2. Nanoimprint mold

In NIL, the minimum pattern replicable is only limited by the pattern size on the mold because of its physical replication mechanism. It is crucially important to fabricate the mold with high precision. The NIL molds are usually made of rigid materials, such as Si, SiO_2 and Ni [28, 29] considering not only hardness and durability but also compatibility with conventional nanofabrication techniques. Additionally, small thermal expansion coefficients are required in thermal NIL to avoid pattern distortion and alignment inaccuracy. The commonly used fabrication process of the Si or SiO_2 mold is illustrated in Figure 7. A resist layer is firstly spin-coated on the Si or SiO_2 surface and defined desired mold patterns by lithography, such as photolithography for microscale features or electron beam lithography for nanoscale features. For ultra-high resolution, there are also other patterning technologies such as EUV lithography, AFM tip-based direct writing, X-ray lithography, directed self-assembly process, and interference lithography for large-area periodic features. After the removal of the residual layer, a layer of metal is deposited over the patterned resist, followed by a lift-off process to maintain a patterned hard mask on the substrate. Si material in the exposed region is etched away by a RIE process, which produces relief structures for NIL. For UV NIL, quartz mold is widely used where UV transparency is a must.

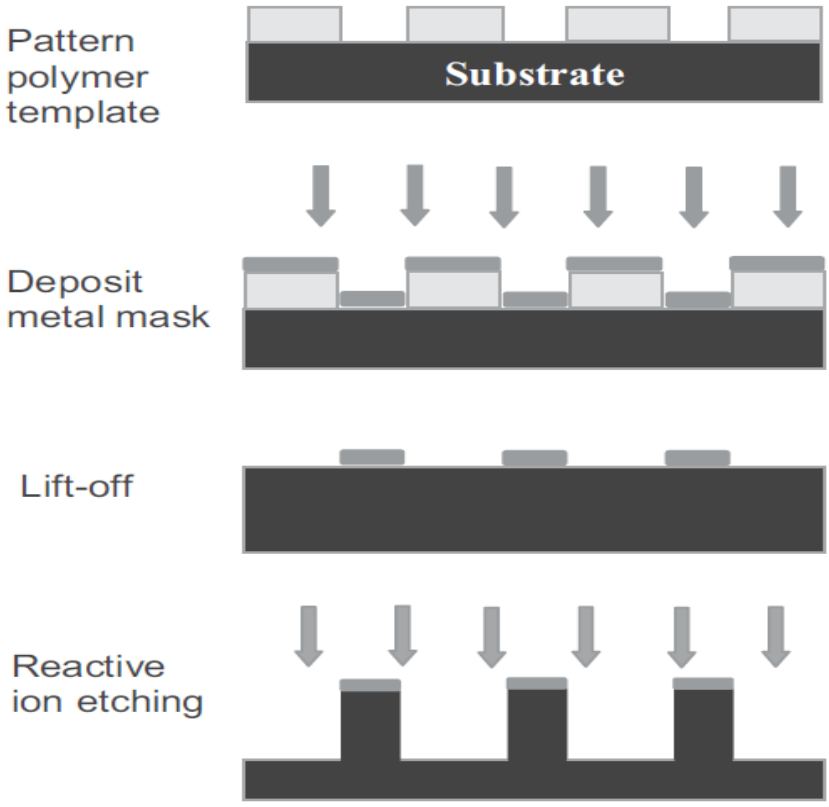

Figure 7 Schematics of the Si mold fabrication [29].

In some cases, there are alternative materials used for NIL mold, including diamond [30, 31], silicon carbide [32], even some polymeric materials that have a sufficient Young modulus typically in biomedical applications, such as poly(dimethylsiloxane) (PDMS) [33] and the cured thermal-set polymers [34, 35]. Small diameter, single-walled carbon nanotubes is used as NIL mold by Feng hua et al [36], which achieves feature sizes as small as 2 nm as shown in Figure 8. It is comparable to the size of a single molecule.

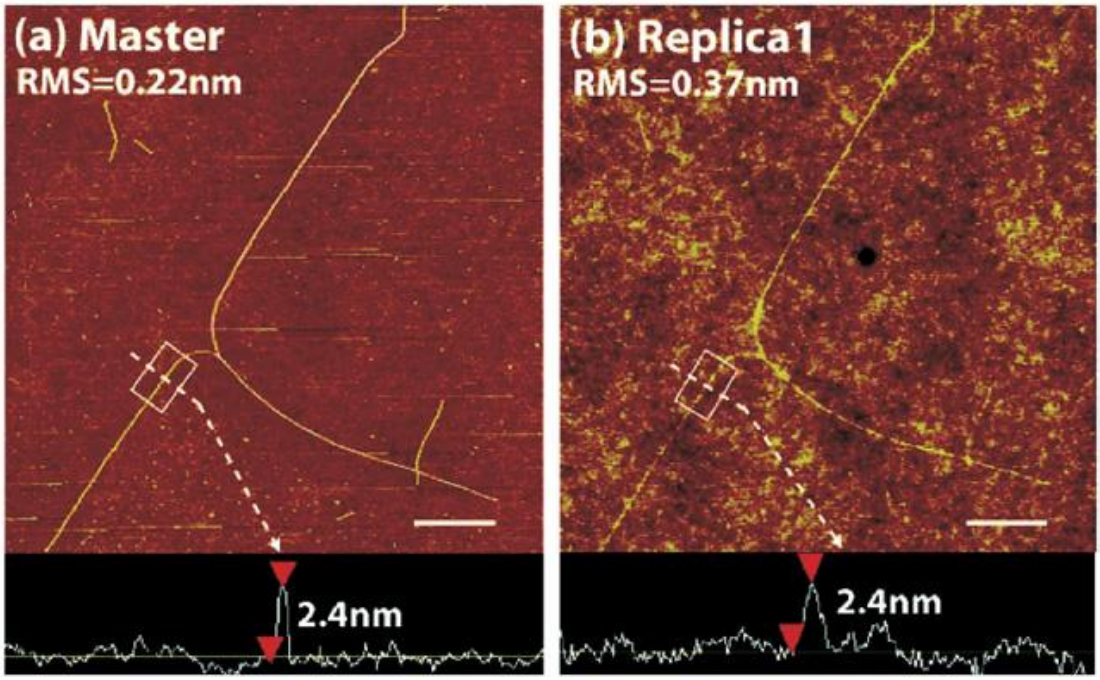

Figure 8 AFM images of a SWNT master and polymer nanostructures replicated by imprinting using the SWNT master [36].

There is also a variety of nanoimprint templates commercially available with dimensions scales from 25 nm to tens of microns as shown in Figure 9. Micrometer and larger structures can be easily fabricated using commercial photomasks.

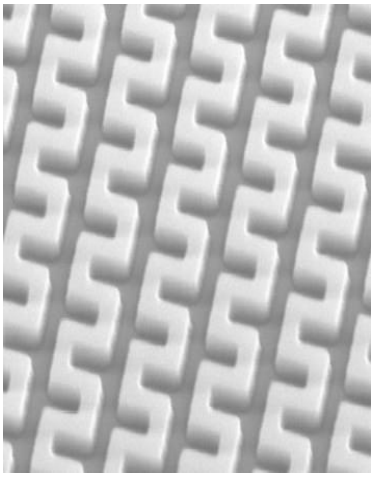

100 nm meander lines (from NILT)

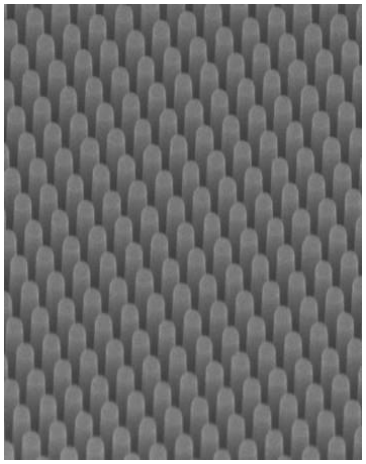

175 nm diameter pillars (from NILT)

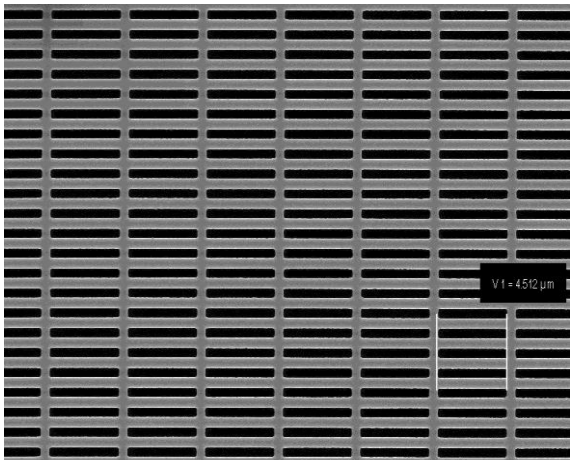

Wire grid pattern (from Eulitha)

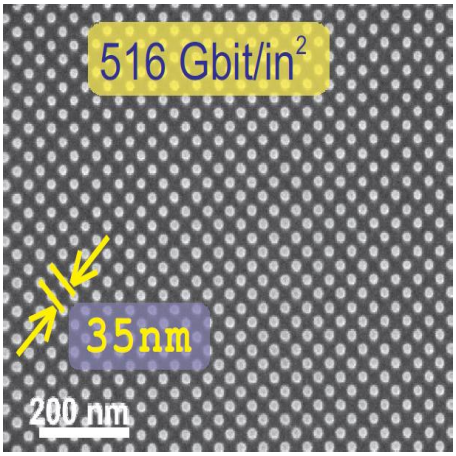

High density nanostructures (from Eulitha)

Figure 9 Commercially available nanoimprint templates.

1.3.3. Nanoimprint mold surfactant coating

A high density of nanoscale protrusion features on the mold surface increases the total contact area between the mold and the polymer layer and therefore leads to a strong surface adhesion of the imprinted polymer to the mold [37-39]. Surface adhesion is a major factor determining the ease of demolding. If the adhesion is strong, the demolding

process can result in significant damage to the pattern or the template. One most widely adopted solution in order to reduce surface adhesion is treating the mold surface with anti-sticking agents coating. This can be done by spin-coating [40] or plasma deposition [41], or by self-assemble molecules (SAMs) deposition [42]. The SAMs process can be achieved either in solvent or in vapor-phase coating.

1H,1H,2H,2H-perfluorodecyltriethoxysilane (FDTS) is a commonly used surfactant which can be deposited on the mold surface either by vapor evaporation or in solvent phase through a silanization process. Formation of a monolayer of FDTS molecules on SiO_2 substrate is shown in Figure 10. The water adsorbed on the silicon surface reacts with the hydrophilic $SiCl_n$ alkylsilanes to form a silanol intermediate and HCl in an irreversible reaction [43-45]. The silanol intermediate has three –OH groups which can either bond to the Si-based mold surface or adjacent molecules to form Si-O-Si bonds through loss of H_2O, resulting in the formation of a monolayer of FDTS SAMs on the surface to create a low-energy surface [46].

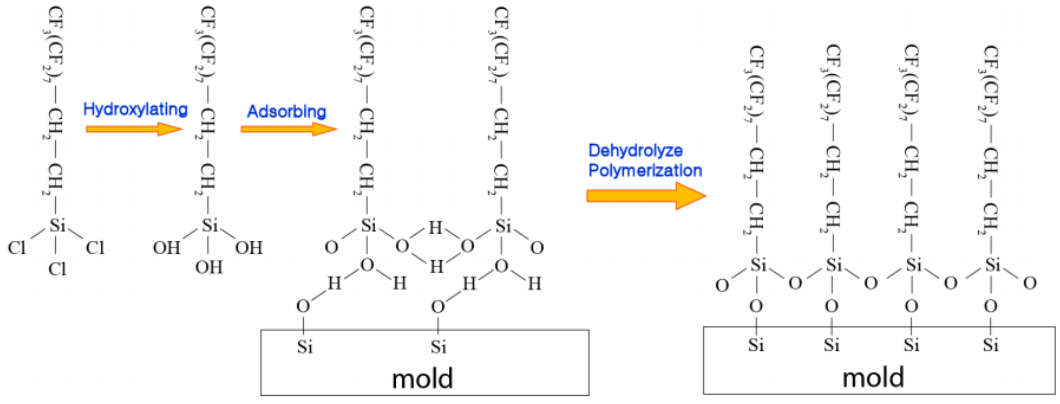

Figure 10 Formation of a monolayer of FDTS molecules on SiO_2.

1.3.4. Nanoimprint resist

A suitable nanoimprint resist material is required to allow for easy deformation under an applied pressure and solidification to preserve the pattern of the impression. Therefore the resist material can be a thermal-plastic polymer, thermal setting polymer if its liquid precursor is used before NIL, or low-viscosity precursor which can be cured either thermally or by UV light.

In thermal NIL, typically thermal plastic materials are used as the imprint resist. Considering the typical deformation behavior of a thermal plastic polymer (Figure 11) [47], the glass transition temperature (T_g) is defined as the onset temperature for molecular motion in polymers. At a temperature below T_g, the polymer is in a glassy state without any motion of polymer chains. Above T_g, local motion of polymer chain segments takes place and the viscosity of the polymer decreases as the temperature increases. With a further increase in temperature, motion of entire polymer chain takes place and the polymer is melted to the viscous liquid flow state. It is perceived that 70–80 ℃ above the T_g of the material is an optimal imprinting temperature which can be used to acquire excellent imprinting patterns.

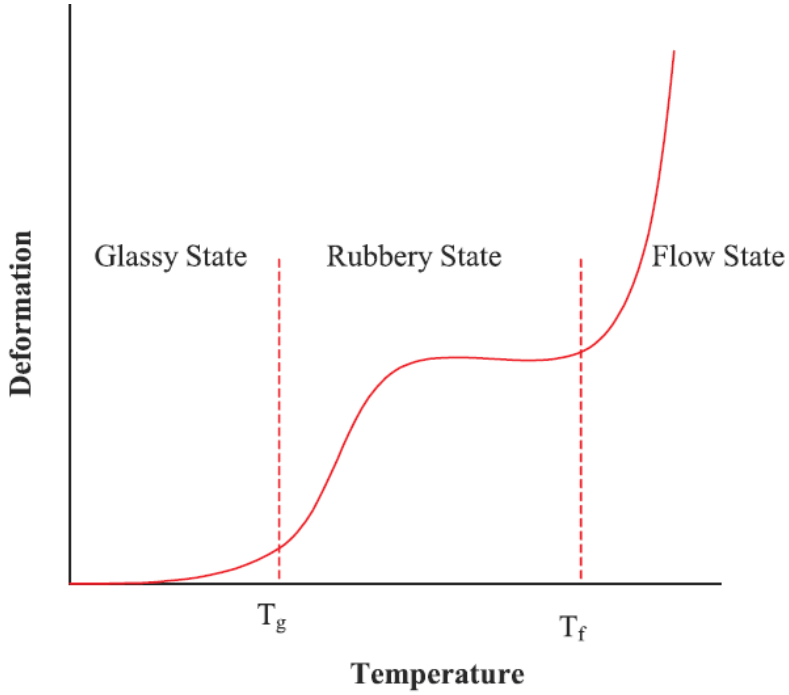

Figure 11 Typical deformation behavior of thermal plastic polymers as a function of temperature [47].

For many applications, a lower temperature in processing is desirable, which refers to a lower T_g of material used. Many factors increase the T_g value including intermolecular forces, branching, cross-linking, and bulky and stiff side groups. The molecular weight of the polymer chain has a significant impact on the viscosity. Polymers with lower molecular weight than the so-called critical molecular weight (M_c) can be imprinted at lower temperature. Therefore linear chain polymers with low molecular weight typically have lower T_g. However, a low-T_g material imprinted pattern is also unstable and tends to decay at temperatures close to the imprinting temperature. This is a trade-off between the imprint temperature and thermal stability. Above all, a

proper material needs to be selected with consideration of these factors. There are commonly used imprint materials including poly(methyl methacrylate) (PMMA), polycarbonate (PC), polystyrene (PS) and etc.

For UV NIL, the resists commonly are UV-curable liquid precursors. The liquid state of UV resists naturally satisfies the low viscosity and Young's modulus requirements. A UV resist is essentially composed of three basic components: a monomer (or oligomer), a cross-linking agent and a photo-initiator. The monomer can either be an acrylate [48, 49] or epoxy [50-55]. The cross-linking agent is a molecule used to make the polymer chains cross-linking and provide mechanical stability because of its larger number of functional groups than that of the monomer. The photo-initiator is used to initiate the polymerization reaction by activating the functional groups. Many companies such as Nanonex, Micro Resist Technology, AMO, MII and etc. have provided commercial resists for UV NIL.

1.3.5. Pattern transfer

Figure 12 illustrates two ways in pattern transfer to the substrate. After patterning, the polymer residual layer is removed by oxygen RIE and the remained polymer patterns can serve as a resist template to transfer pattern to the underlying substrate. Both positive and negative mold pattern can be replicated on the substrate depending on the ways of subsequent pattern transfer. For the direct transfer, the polymer patterns are used as a mask to provide Si/SiO_2-RIE etch resistance. Si material in the exposed region is etched away by a RIE process, which directly transfer reverse mold pattern to the underlying

substrate. For the indirect transfer, a layer of metal is evaporated over the patterned resist, followed by a lift-off process to maintain a reversely hard mask on the substrate. This hard mask is used in etching process to produces relief structures on the substrate. In this way, the same mold patterns can be replicated exactly on the substrate. This versatile pattern replication makes NIL more flexible and attractive.

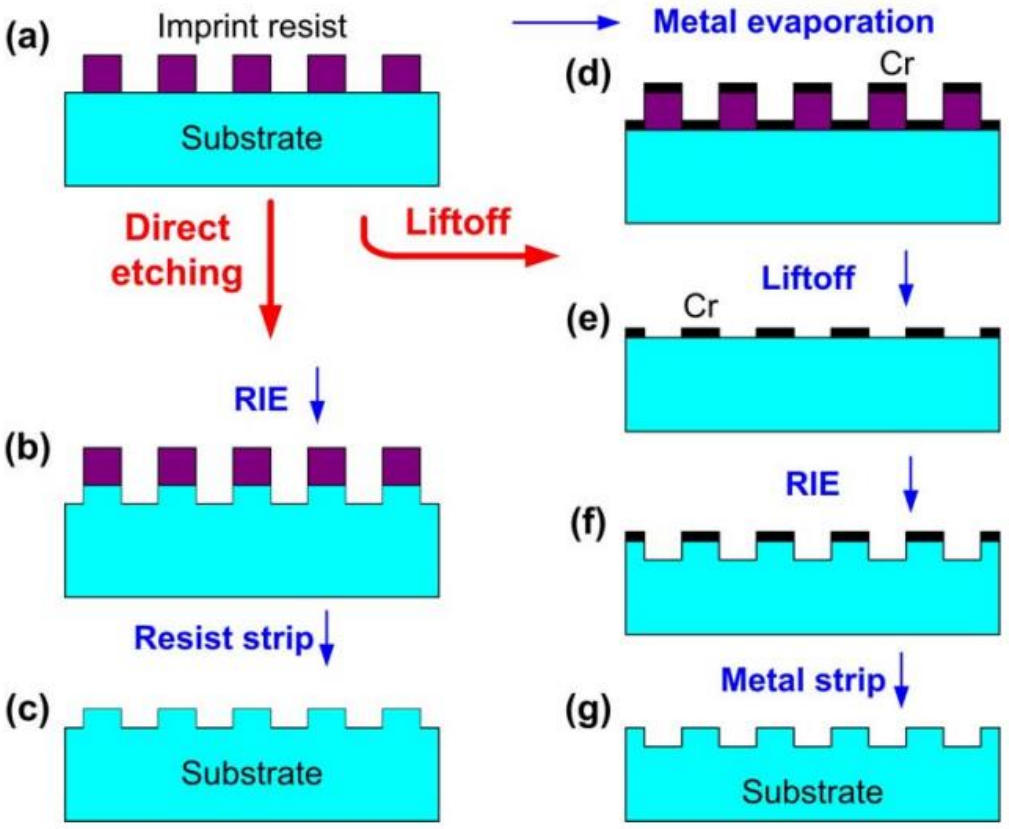

Figure 12 Two ways for pattern transfer to the substrate.

1.3.6. NIL applications

NIL is a promising next generation lithography technique, which can be applied in many applications because of its high resolution, low cost and easy fabrication. It has been widely used in many fields of not only nano-electronics, but also nano-photonics and biomedical sciences, typically including tunable grating filter [56], data storage [11, 18, 57, 58], nano-electronic devices [11, 15, 16, 59, 60], optical devices [18, 61-65], photo detector [66], and bio chips [67, 68].

1.4 Thesis Organization

The primary objective of this study is to propose new schemes to overcome the limitations in the throughput and the density of pattern defects of current NIL process. The development focuses on exploring new methods and material beyond conventional nanoimprint by utilizing three factors: mold, the interface between mold and resist, and resist. The mold used in NIL plays the same role as the photomask in photolithography. The second chapter of this thesis presents a synergistic thermal and UV nanoimprint lithography (STUV-NIL) mold, which combines thermal and UV imprints into one module by using a transparent mold with an integrated heater. Chapter three investigates the thermal behavior of polycarbonate gratings after thermal annealing for large-area and high throughput application. Since NIL replies on close contact between the mold and polymer layer, surface adhesion between the mold and the resist directly determines the ease of demolding and affects the pattern quality. Chapter four takes advantage of PC residual layer to treat the mold surface as a new low surface energy surfactant. In UV

NIL, polymerization shrinkage stress in polymer resist contributes to the overall demolding force, resulting in pattern decay after demolding. Chapter five investigates and optimizes the chemical composition of a new UV resist by adding spiro-orthocarbonate to hinder the polymerization shrinkage in UV NIL. The last chapter of this thesis will give a conclusion of this work.

CHAPTER II

A SYNERGISTIC THERMAL AND UV NANOIMPRINT LITHOGRAPHY (STUV-NIL)

2.1 Introduction

As discussed in the introduction section, nanoimprint lithography (NIL) has been envisioned as one of the next generation lithography techniques with high throughput and low cost since the first demonstrations on thermal and UV NIL [9, 11, 26]. However, both conventional thermal and UV NIL have several limitations. Conventional thermal NIL commonly imprints thermal-plastic polymers upon heating to 70–80 ℃ above the glass transition temperature (T_g) of the used materials for a significant reduction in the resists' viscosities. A long process cycle time is necessary in thermal NIL for the heating up and cooling down stages and hence leads to a limitation in the throughput of the NIL process. In addition, high imprinting temperature puts greater demands on the equipment setup and therefore increases the cost. UV NIL is usually imprinted at room temperature because the lower viscosity of UV curable resists easily ensures full filling of the features of the mold. However, a big challenge in UV NIL is a high rate of defect generation during the demolding process [28, 29, 69]. A lot of efforts have been devoted to conquer these problems in thermal and UV NIL. In this study, we present a synergistic thermal and UV nanoimprint lithography (STUV-NIL) by using a transparent

nanoimprint mold with an integrated heater in order to combine the advantages of both thermal and UV NIL together and meanwhile overcome the respective limitations.

2.2 A Designed Nanoimprint Mold with an Integrated Heater

The designed nanoimprint mold with an integrated heater is constructed by an indium tin oxide (ITO) layer deposited on the fused silica mold with metallic films for electric contact (Figure 13). The ITO heater is conductive and capable of providing excellent optical transparency in visible and UV light wavelength range. Figure 14(a) and (d) show an ITO layer (red part) is coated on the top of the mold with metal stripes (blue part) patterned on two edges of the ITO layer. Once applying power to the electrodes, electric current is generated through the conductive ITO layer. Because of Joule heating, the underlying mold can be heated to a high temperature. Another meander-shaped heater is designed on the mold as illustrated in Figure 14(b) and (e). For this design, the mold is firstly masked using masking tapes (Scotch) to form the desired pattern. After the ITO layer deposition, the removal of the masking tapes forms patterned ITO structure, followed by two electrodes patterned at both ends. The patterned heater allows higher resistance or voltage. The third one is a meander-shaped heater covering the whole layer (Figure 14(c) and (f)). This design keeps the resistance large while maintaining uniform heating.

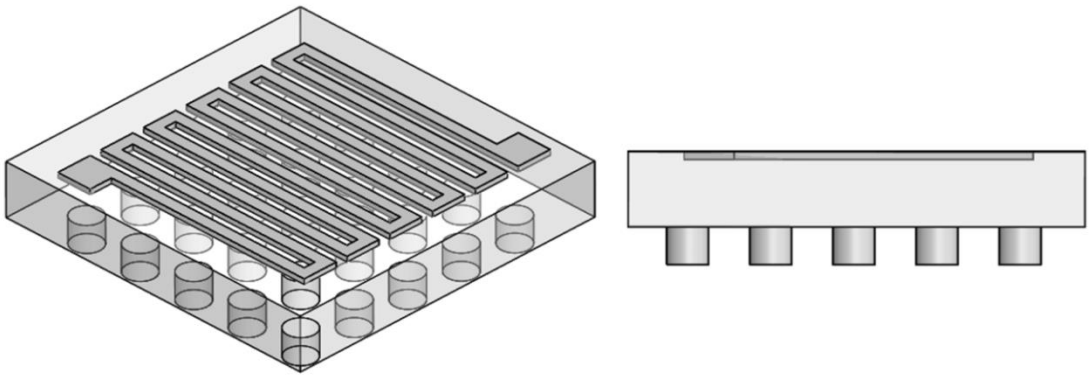

Figure 13 Schematics of integrated transparent metal oxide resistor on transparent quartz or fused silica mold.

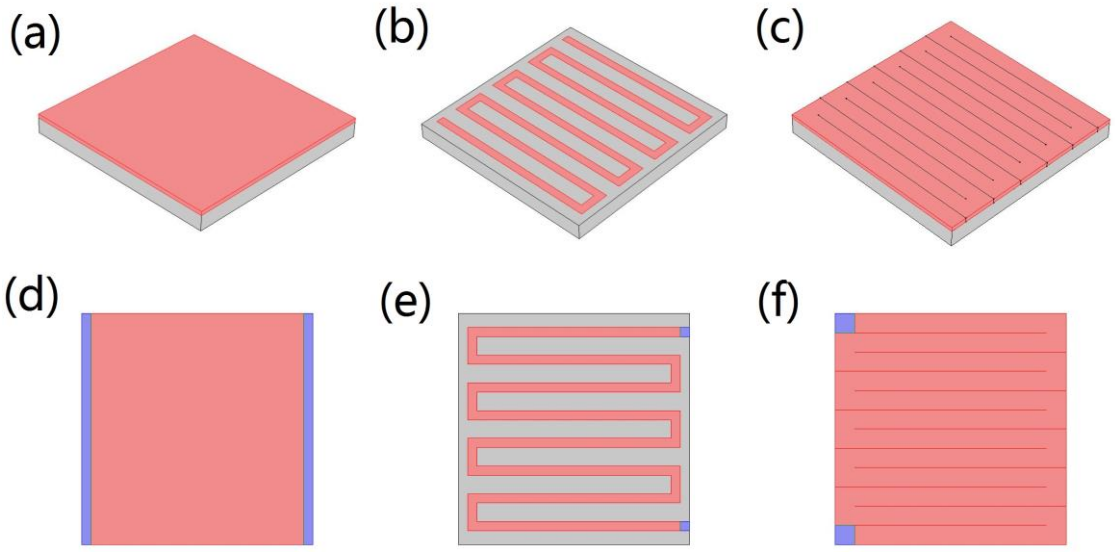

Figure 14 Schematics of three heater-integrated mold designs: (a) uniform layer heater; (b) meander-shaped resistor as a heater; (c) meander-shaped heater covering the whole layer. (d), (e), and (f) are top views of (a), (b), and (c), respectively.

For the imprint process with the STUV mold, Figure 15 shows schematics of thermal NIL process with heating ITO layer on mold. The STUV mold is brought into close contact with the thermal-plastic polymer resist on the substrate. Upon heating up to above its T_g by applying a power to the heater, the polymer melts and reflows to fill the features of the mold under a suitable pressure. After a certain holding time to allow sufficient polymer reflow for full filling of the features, the mold is cooled down to the ambient temperature for the patterns to solidify. Then the mold is separated, while the patterns are maintained on the substrate.

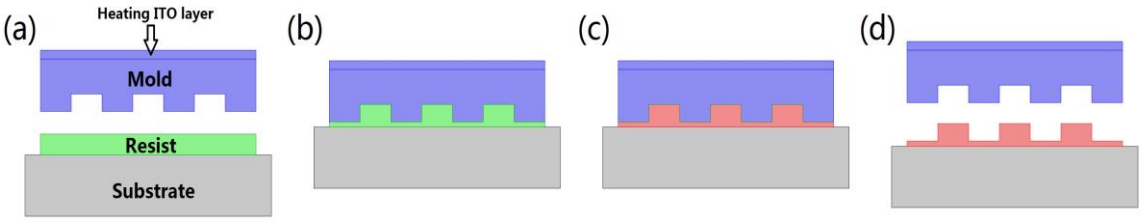

Figure 15 Thermal NIL process with heating ITO layer on mold.

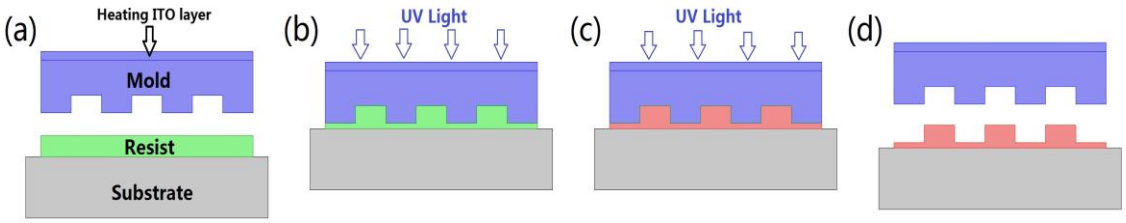

Figure 16 Synergistic thermal and UV NIL process by nanoimprint mold with integrated heater.

Alternatively, ITO can be replaced by other transparent and conductive oxides, such as fluorine doped tin oxide (FTO) and aluminum doped zinc oxide (AZO). The transparent property of these oxides allows UV light to transmit the quartz mold to cure the UV-curable resist, and the heating property provides a higher temperature rather than the ambient temperature. Therefore, thermal and UV curing can be achieved simultaneously. The process schematics are shown in Figure 16. The mold is firstly imprinted in the UV curable polymer on the substrate under a low pressure. The low viscosity of the resist easily ensures full filling of the features of the mold. The whole assembly is then heated up to a high temperature by applying a power to the electrodes. While maintaining the temperature and pressure, the assembly is exposed to a UV light. The UV-induced polymerization process converts the liquid resist patterns to solid form; this polymerization process can be accelerated under a high temperature. Additionally, the demolding process at a temperature higher than room temperature may also help in reducing mold-resist adhesion and hence defect generation.

2.3 Simulation

For the heating process simulation, COMSOL Multiphysics is used in this study. In the model, a whole ITO layer with a thickness of 200 nm is coated on a 25 mm $\times$ 25 mm $\times$ 1 mm mold as the model in Figure 14(d). Two electrodes with dimensions of 1 mm $\times$ 25 mm are patterned on two edges of the ITO layer.

Firstly, a constant voltage of 2.75 V is applied to the electrodes, and the trend of temperature with time is obtained as simulated in Figure 17. The temperature rises

dramatically in the beginning 200 s, and then the increase gradually becomes sluggish and finally reaches an equilibrium state. After 1000 s, the temperature is stable and fixed at 100 ℃.

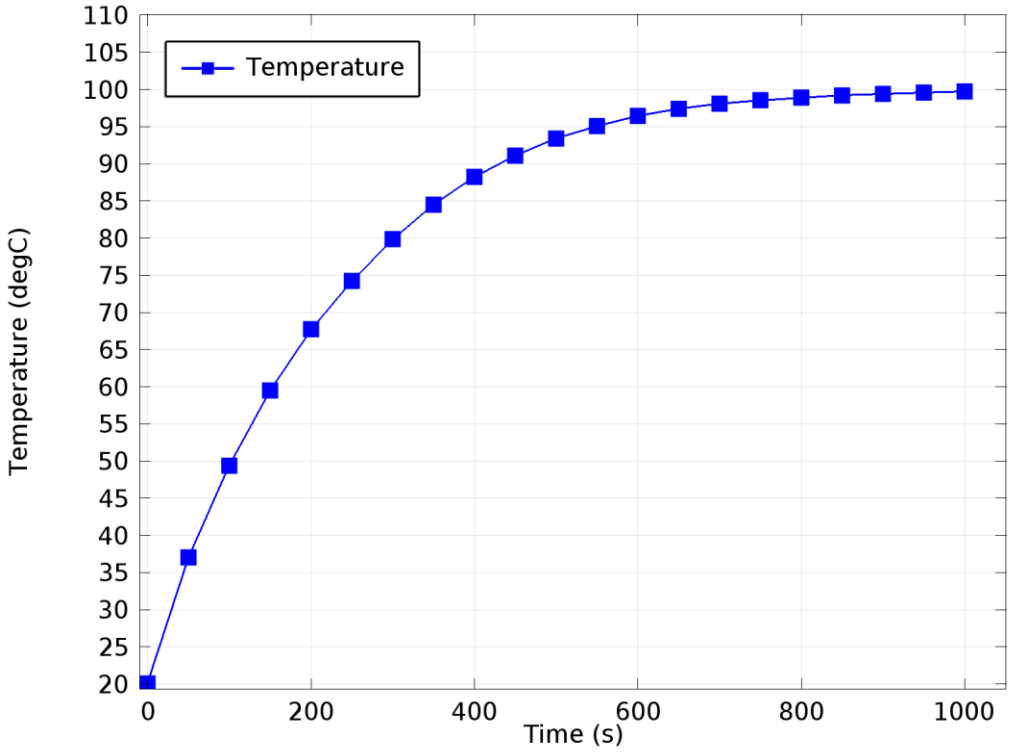

Figure 17 Simulated temperature of the mold as a function of heating time with the uniform layer heater for reaching 100 ℃.

The equilibrium is obtained by the balance between heat generation by Joule heating and heat dissipation by convection. The power of heat generation is determined by the applied voltage and the resistance of the ITO resistor. The power of dissipation is determined by the heat transfer coefficient of air and the temperature difference between

the mold and environment. We use 5 W/(m^2·K) as the value of heat transfer coefficient, which stands for natural air convection. For the heating process, at first, the power of heat generation is larger than that of heat dissipation because of the small temperature difference between the mold and environment. The resultant heat accumulation leads to a gradual increase in the mold temperature. The higher the mold temperature is, the larger the power of dissipation would be. When the power of dissipation is increased and equaled to the power of generation, an equilibrium state is obtained, which leads to a stable temperature.

Secondly, a series of different voltage values are given as parameters, and the relationship of stable temperature and input voltage is simulated as shown in Figure 18. The result suggests that the process temperature can be precisely controlled by adjusting the input power, which meets the imprint temperature requirements for various resist materials in NIL processes.

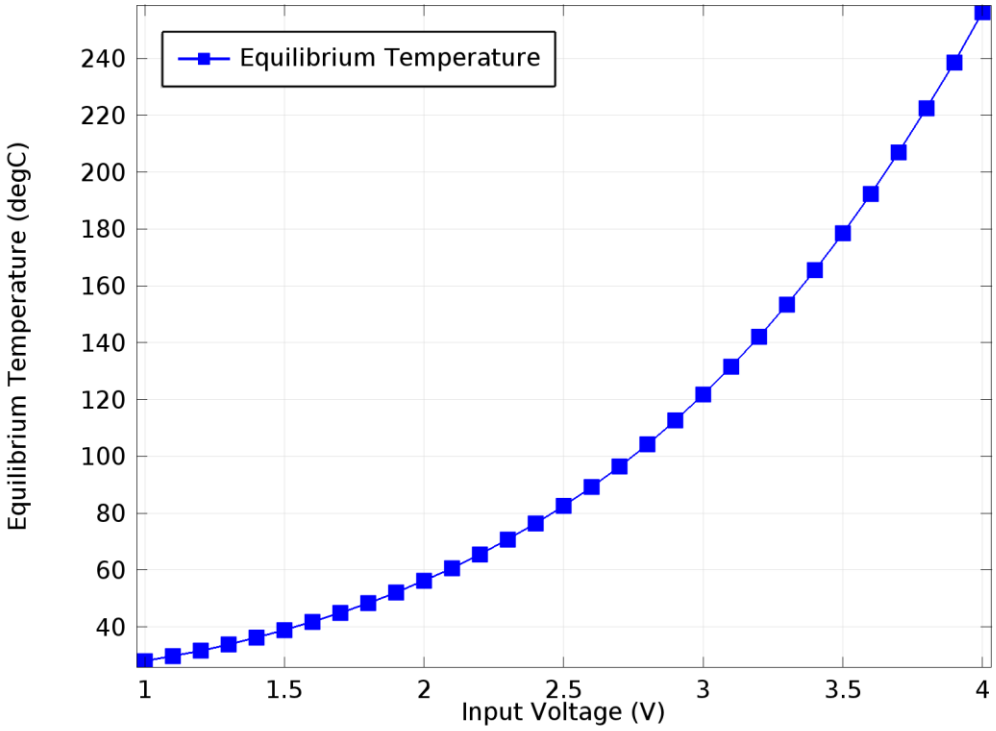

Figure 18 Temperature-voltage curve of the mold with uniform layer heater.

The NIL process could be conducted when the mold reaches the target stable temperature. But as seen in Figure 17, it costs about 1000 s to reach a stable temperature at 100 ℃. For a higher stable temperature, it takes even longer time for the thermal cycle, which significantly limits the throughput of fabrication. Therefore a faster heating method is demanded. To meet the purpose of fast heating, a two-step biasing is used in the simulation, which is a higher voltage pulse for quick heating followed by a low voltage bias to maintain the temperature. The temperature of the mold as a function of heating time for quick heating is simulated in Figure 19, which presents the targets of 60 ℃ for STUV-NIL and 150 ℃ for thermal NIL. In Figure 19(a), 15 V is applied for the first

3 s for a rapid heating, followed by applying a small voltage of 2.05 V. The value of 2.05 V corresponds to the stable temperature 60 ℃, which is obtained in Figure 18. In Figure 19 (b), after a fast heating of 15 V for the first 8.5 s, a corresponding voltage of 3.27 V to 150 ℃ is applied. For rapid heating, a high voltage or power input is given firstly. When the temperature approaches to the desired value for NIL fabrication, the input is then changed to a smaller voltage corresponding to the temperature in equilibrium state. The simulation results show that the time needed to reach a stable temperature for NIL can be shortened to tens of seconds. Rapid thermal cycles in practical experiments lead to a relatively high throughput in nanoimprint.

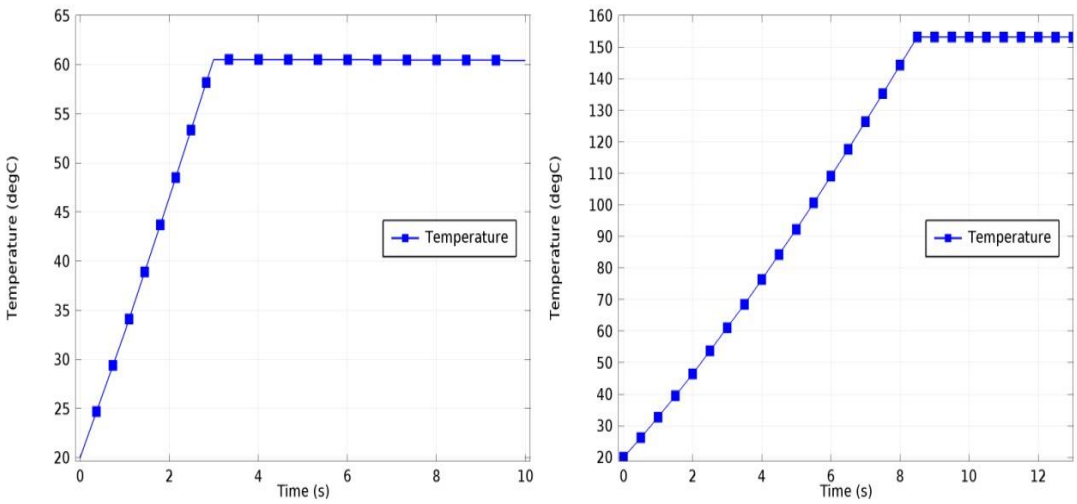

(a) (b)

Figure 19 Simulated temperature of the mold with uniform layer heater as a function of heating time with dynamic input power: (a) 60 ℃ for synergistic thermal and UV NIL; (b) 150 ℃ for thermal NIL.

2.4 Experimental

The fused silica molds with dimensions of about 10 mm × 10 mm × 1 mm are prepared with desired micro-features by lithography and RIE processes. A layer of ITO thin film with a thickness of 200 nm was coated on each mold using electron beam deposition, followed by annealing the device in a 500 ℃ N_2 convection oven for 5 min. The resulting sheet resistance of the annealed ITO layer was ~8 Ω/square. Two copper tapes (1 mm width and 0.05 mm thick) were used as electrodes on two edges of the ITO layer for smooth generation of electric current through the ITO layer for uniform Joule heating. Electrical wires were attached to the copper stripes to form connections to external control circuits. The power source was supplied by RIGOL DP1308A Programmable DC Power Supply. The heater surface temperature was detected by OMEGA OM-DAQPRO-5300-UNIV Data Recorder associated with PT100 RTD. As a consequence, the mold can be heated up and maintained constantly at an elevated temperature.

For NIL, the mold was immersed into heptane solution with 1H,1H,2H,2H-perfluorodecyltrichlorosilane (FDTS, TCI Co.) for 10 min for the surface treatment, which is prepared for easy demolding. A layer of UV nanoimprint resist was spin-coated on a SiO_2 substrate for STUV-NIL and a layer of thermal nanoimprint resist was coated for thermal NIL.

2.5 Results and Discussion

The relationship curves between the temperature and input power in air ambient condition (Figure 20(a)) and in manual hydraulic press machine (Figure 20(b)) were obtained. It is shown that the temperature is proportional to the input power in both figures. A larger input power is required in manual hydraulic press machine for the same temperature because of its larger dissipation through platens.

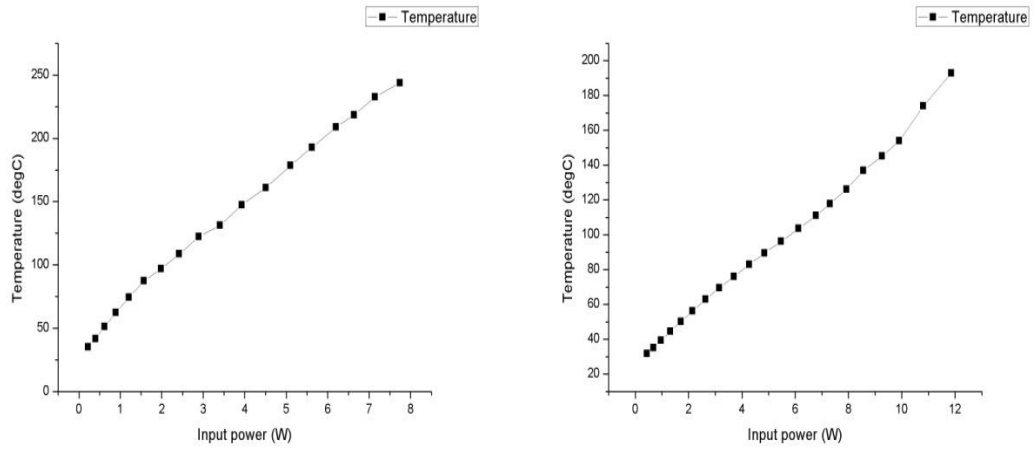

(a) (b)

Figure 20 Temperature-power relationships in (a) ambient condition and (b) manual hydraulic press machine.

As discussed in the simulation, a dynamic input is proposed for fast heating process. In experiments as described in Figure 21(a), a large input of 15 W was applied for the beginning 7 s, followed by using a corresponding 2.4 W for 60 ℃. It is demonstrated that a stable 60 ℃ is reached rapidly within 10 s in the manual hydraulic

press machine. In Figure 21(b), it takes about 30 s to reach a constant 140 ℃. In the process, 15 W is applied in the first 22 s, which is then followed by a corresponding power of 8.8 W. The time can be further shortened by using larger power than 15 W in the first stage for faster heating. Above all, it is verified that the thermal cycles can be shortened to the order of 10 s, which results in effective improvement in the throughput.

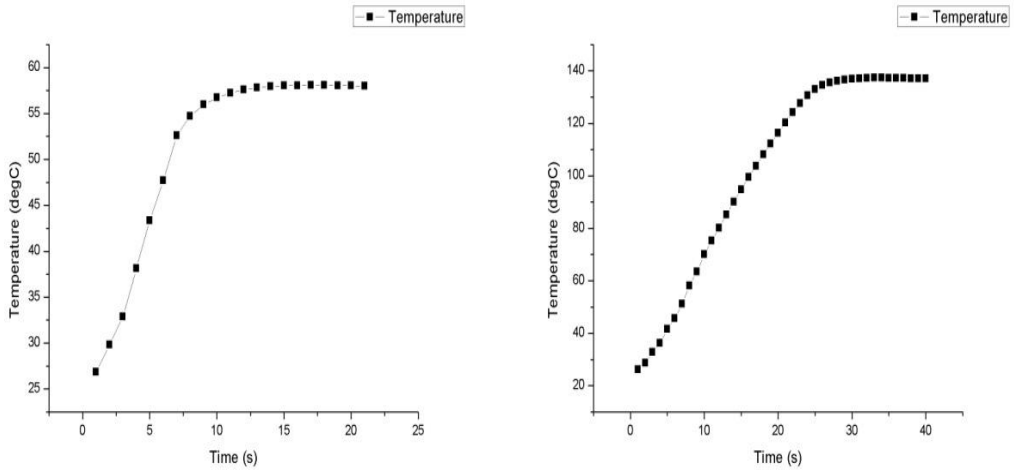

(a) (b)

Figure 21 Experimentally measured temperature of the mold as a function of heating time with dynamic input power: (a) 60 ℃ and (b) 140 ℃.

The FDTS-treated mold is applied in STUV-NIL to imprint patterns on the resist-coating substrate. UV curable imprint resist is spin-coated on a substrate and pressed by the mold with a low pressure. While maintained being pressed, the whole assembly is heated by applying a 2.4 W to achieve a 60 ℃ stable temperature, followed by UV

irradiation for curing. The wavelength used for UV curing is 365 nm and the exposure dose is 7.1 mW/cm^2. After cured for 1 min, the mold is released and the resist replicated the pattern from the mold as shown in Figure 22. The SEM image suggests good quality of curing for the resist under thermal energy and UV light simultaneously. This means STUV-NIL can be an effective NIL technique for fabricating micro- and nanostructures.

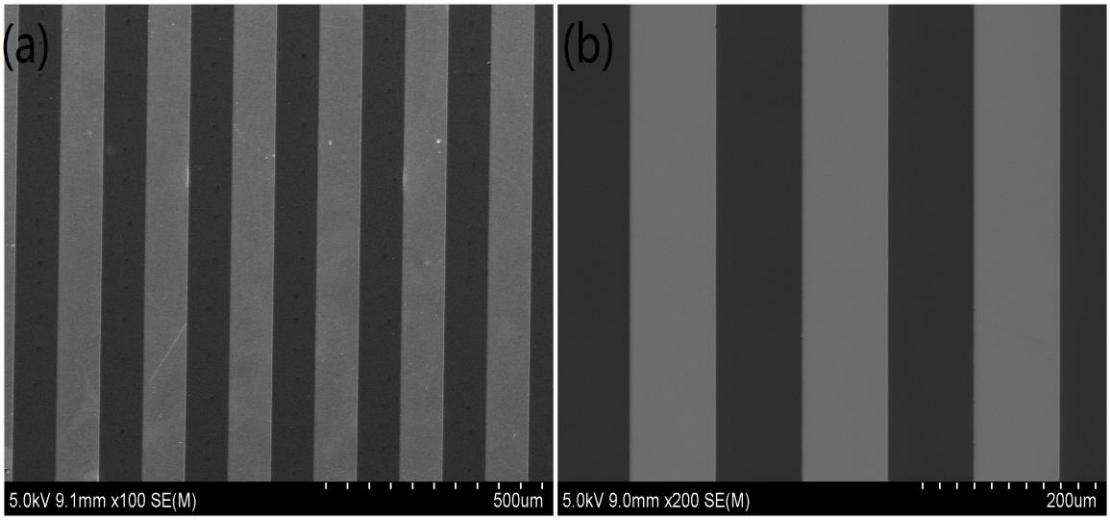

Figure 22 SEM images of (a) imprinted resist by synergistic thermal and UV NIL with integrated heater at about 60 ℃ and (b) the imprint mold.

For thermal NIL only, the mold is brought into close contact with the thermal nanoimprint resist coating substrate. The whole assembly is heated by applying a 8.8 W power to achieve a 140 ℃ stable temperature. When the desired temperature is reached, the mold is pressed into the underlying resist under a pressure of 5 MPa in the manual hydraulic press machine. After maintaining the temperature for 5 min, the assembly is

cooled down to the room temperature (RT). Then the mold is released from the substrate and the solidified patterns are formed on the substrate, which is shown in Figure 23. The high-quality pattern in the SEM image also indicates the STUV mold can be effectively used in thermal NIL only.

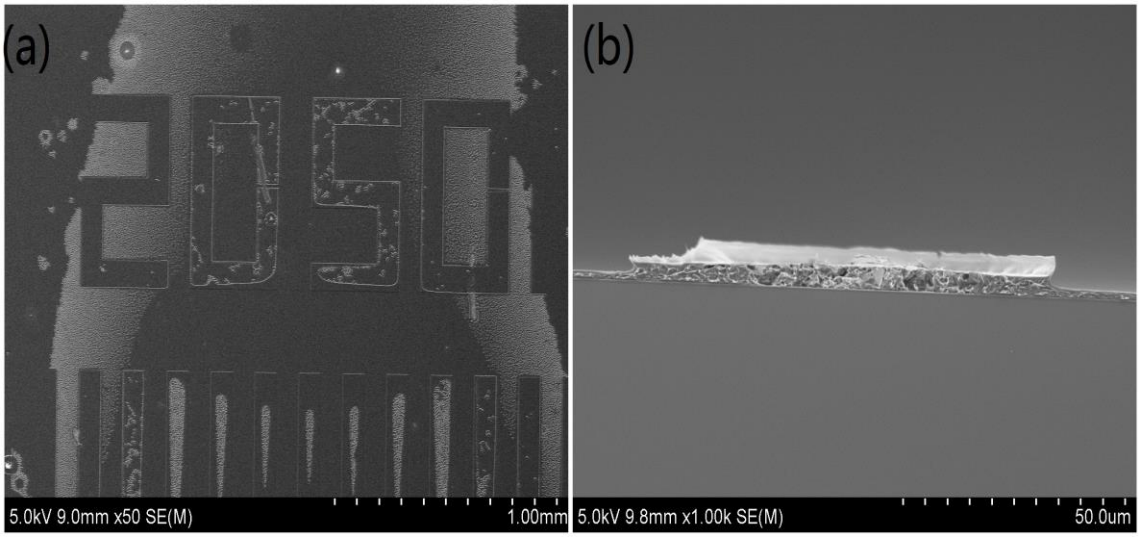

Figure 23 SEM images of (a) imprinted resist and (b) cross-section of imprinted resist by thermal NIL with integrated heater at about 140 ℃.

2.6 Summary and Discussion

In summary, we have demonstrated a new STUV-NIL technique by integrating a transparent mold with a transparent heater. The feasibility of STUV-NIL technique has been verified by simulations and experiments. Micro-scale patterns with high quality have been fabricated by STUV-NIL, which may lead to improvements in defect and throughput issues.

For conventional thermal and UV NIL, large-volume setups are required respectively in terms of different imprinting conditions, i.e. heating setups and UV light sources. The new STUV-NIL can combine these two NIL techniques into one module while satisfying all requirements for different nanoimprint modes. This design would significantly simplify the expensive NIL setups and therefore reduce the cost.

For conducting thermal NIL only with the module, it only takes 30 s to heat the mold to a target temperature of 140 ℃. Compared with several minutes in conventional thermal NIL, the throughput is greatly improved and enhanced. Additionally, in conventional thermal NIL, the whole press platens (made of Al with a cylindrical volume of $2 \times 3.14 \times 5^2 \times 2$ cm^3) need to be heated up during nanoimprint process. In STUV-NIL, it only needs to heat the SiO_2 mold with a volume of $10 \times 10 \times 1$ mm^3. Considering the differences of specific materials heat capacity and density, it needs 3000 times more energy for conventional thermal NIL process than that in our local heating technique to conduct the curing process at the same temperature. The capability of saving energy and cost makes the STUV-NIL to be a potential technique for mass production commercially. Moreover, the conventional thermal NIL cannot implement step-and-repeat mechanism for nano-patterning over a large substrate because subsequent NIL requires heating to above the glass transition temperature (T_g) of the polymer resist, which will inevitably destroy the nanostructures formed in preceding nanoimprints. In STUV-NIL, the limited heating area makes it feasible to achieve the step-and-repeat capability in thermal NIL for large-area polymer patterning.

In STUV-NIL, it allows UV NIL to be done at a high temperature, which leads to a faster curing and more completed polymerization. This shortened the exposure time and thus improved the throughput. Also, demolding at an optimal temperature higher than room temperature would help to reduce the demolding force, and hence reduce defect generation [70]. In the STUV-NIL technique, the demolding temperature can be precisely controlled to the optimal value for better pattern quality. Moreover, the STUV-NIL can simplify conventional imprint methods through one-step processing for some special materials, such as SU8, which needs both heat and UV light treatments when imprinted [71]. Therefore the throughput is enhanced.

In all, this new technique has numerous advantages over conventional thermal and UV NIL in improving throughput and reducing defects. We expect the STUV-NIL can bring about greater versatility in NIL processes.

CHAPTER III

EXCEPTIONAL THERMAL STABILITY OF THERMOPLASTIC POLYMER NANOSTRUCTURES

3.1 Introduction to Thermal Behavior of Thermoplastic Polymers

Nanoimprint lithography (NIL) is a high throughput and low cost patterning technique, which has been developed to overcome the resolution limit of photolithography [72]. NIL forms nanoscale patterns in a thermoplastic polymer film by deforming the polymer under high pressure at an elevated temperature with a hard mold. In recent years, both UV [26] and thermal [11] nanoimprint have demonstrated sub-10 nm resolution. However, there still remain various issues for the acceptance of imprint-based technology in industrial applications. For thermal NIL, a critical issue in terms of pattern stability is related to internal stress relaxation at temperatures close to or even below the glass transition temperature (T_g) of the polymer after imprinting [73].

The reflow behavior of polymer micro- and nanostructures fabricated by thermal NIL has been widely investigated [74, 75]. In general, dramatic thermal expansion can be observed by thermal annealing of the polymer patterns at temperatures above T_g, and with extended annealing, the pattern shape was no longer maintained due to excessive polymer flow. In this work, we observed and investigated the unusual reflow behavior of polycarbonate gratings after thermal annealing.

3.2 Experimental

Polycarbonate is a widely used transparent amorphous thermoplastic material with a glass transition temperature (T_g) of 150 ℃. Polycarbonate resin with average molecular weight (M_w) of 30900 was supplied by Scientific Polymer Product Inc.; 0.6 wt%, 1 wt% and 2 wt% polycarbonate solutions were prepared by dissolving polycarbonate powders into cyclopentanone solvent. Figure 24 shows a schematic of polycarbonate nanoimprint and thermal annealing processes: polycarbonate thin films with different thicknesses were obtained by spin-coating the prepared solutions on SiO_2 substrates (Figure 24(a)). Then these polycarbonate films were imprinted by a 600 nm period (50% duty cycle, 190 nm depth) SiO_2 grating mold at 220 ℃ and 5 MPa as shown in Figure 24(b). The residual layers were removed by oxygen reactive ion etching (RIE) treatment after nanoimprint in Figure 24(c). The resultant polycarbonate gratings were characterized by atomic force microscopy (AFM) (Bruker Dimension Icon); different grating heights of 25 nm, 56 nm and 103 nm, respectively, were obtained. Finally these polycarbonate gratings were annealed on a hot plate at 250 ℃ for 30 min to induce polymer reflow in Figure 24(d).

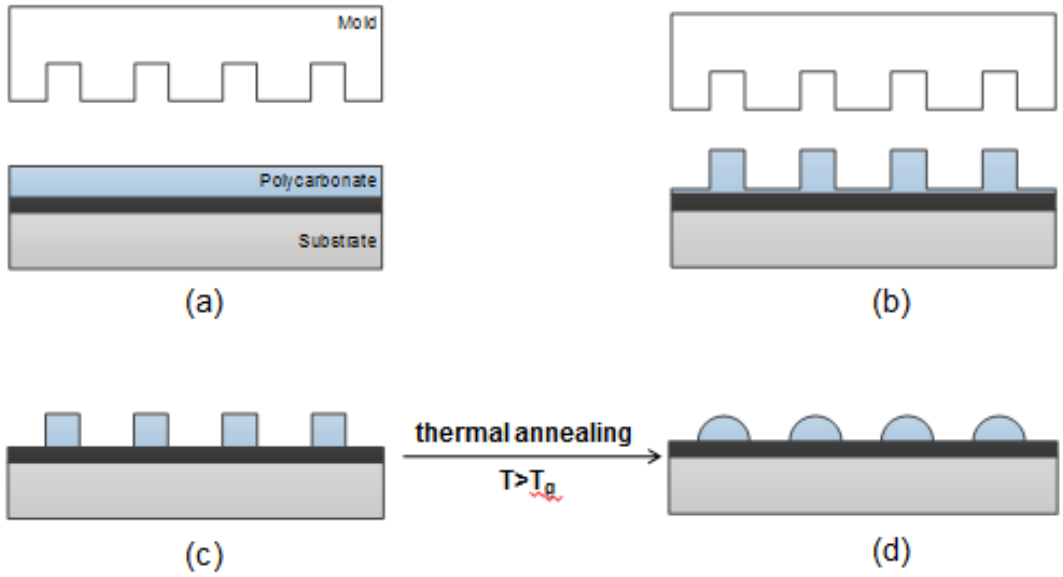

Figure 24 A schematic of polycarbonate nanoimprint and thermal annealing: (a) polycarbonate resist on a substrate; (b) thermal nanoimprint to form polycarbonate nanostructures; (c) oxygen RIE to remove the residual layer after nanoimprint; (d) annealing of polycarbonate nanostructures on a hot plate at elevated temperatures to induce polymer reflow.

3.3 Results and Discussion

The AFM images for polycarbonate nanostructures after 30 min annealing at 250 ℃ are shown in Figure 25. Apparently, Figure 25(a) shows the original 25 nm polymer gratings are piled up with smaller dimensions (~16.67%) than those of the mold. When annealed at a temperature above T_g, the thin PC film would dewet on the substrate resulting in pattern shrinkage.

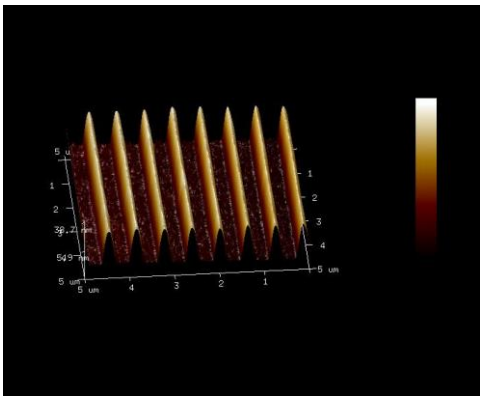

(a)

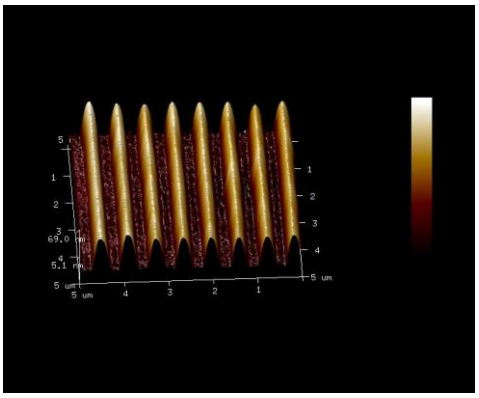

(b)

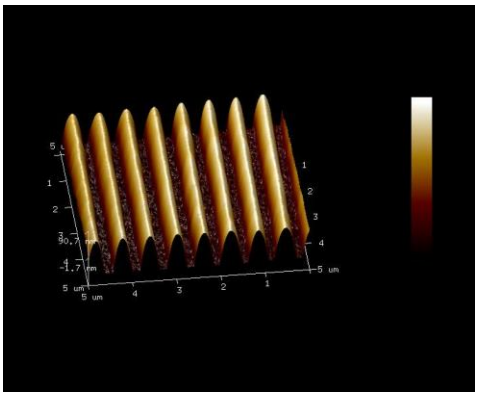

(c)

Figure 25 AFM images for various polycarbonate gratings after 30 min annealing at 250 ℃ with initial thicknesses of (a) 25 nm, (b) 56 nm and (c) 103 nm.

For the same polycarbonate gratings with a height of 56 nm, it was experimentally observed that the annealed polycarbonate patterns tend to stay stable in Figure 25(b). The fact that no change of dimension after annealing clearly shows that the polycarbonate patterns exhibited unusual stability at temperatures well above its T_g. When the gratings height is increased to 103 nm, the annealing tests revealed a very different trend. All polycarbonate nanostructures showed significant diameter increase due to pattern relaxation in Figure 25(c). These results suggested that the polycarbonate thickness determines the final equilibrium state, which can be explained by the mechanism of polymer chain entanglement in the following sections.

3.4 Polymer Chain Entanglement

For low molecular weight polymers, the polymer melt dynamics theory is described by Rouse model (Figure 26(a)). This model based on an isolated polymer chain with low molecular weight polymer in low concentration solution. In Rouse model [76], the low molecular weight polymer chains are described as beads, which are connected by springs in a stochastic background. According to Rouse model, the self-diffusion coefficient of polymer is $D \propto N^{-1}$ and the viscosity $\eta \propto N$, where N is the degree of polymerization.

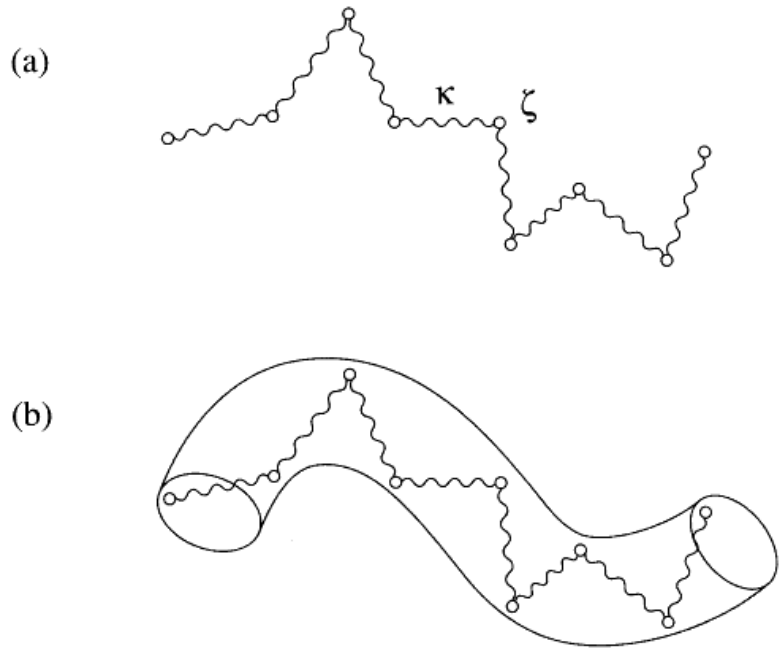

Figure 26 Chain schematics of (a) Rouse model and (b) tube confinement [77].

For polymers with high molecular weight, the theory for polymer melt dynamics is described by reptation model (Figure 26(b)). The reptation model described that a single chain is confined within a tube surrounded by other chains because of polymer chain entanglement. For large molecular weight polymers, the diffusion of a single chain towards the lateral direction of its backbone is limited by the interpenetrating of surrounding polymer chains. The overall diffusion coefficient is reduced ($D \propto N^{-2}$ and $\eta \propto N^{-3.4}$) [78, 79]. The entanglement molecular weight M_e is defined for a given polymer that if $M<M_e$ the Rouse model dominates while if $M>M_e$ the reptation model overtakes the Rouse model. In this work, polycarbonate (M_w=31k) is used with an experimental

and theoretical entanglement molecular weight of 1K [80, 81], which renders 31 M_e for the resist of polycarbonate. Therefore it is well-entangled.

It was demonstrated that the reflow behavior of well-entangled polycarbonate nanostructures exhibit strong dependency on the pattern thickness. Figure 27 illustrated different reflow behavior related to the initial pattern thickness. Three regions – dewetting, stability and relaxation – were observed with increasing pattern thickness. Shallow nanostructures of polycarbonate showed exceptional stability upon thermal annealing at temperatures well above T_g and dewetting can be observed. For relatively thicker nanostructures, although pattern relaxation was observed at the initial stage of the thermal annealing process, stable patterns formed after reaching the "end point" of the reflow, which relied on the initial thickness of the pattern prior to thermal annealing. In addition, a transition region between dewetting and wetting behavior can be identified by careful control of the pattern initial thickness. In this region, no obvious pattern shrinkage or relaxation was observed upon thermal annealing.

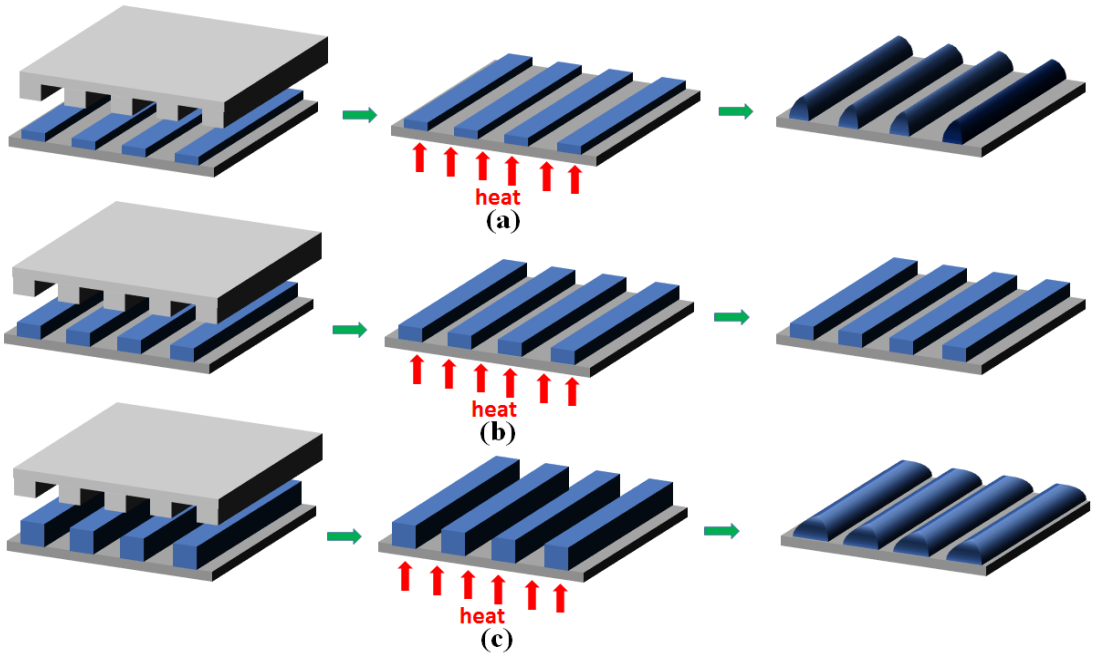

Figure 27 Schematics of reflow behavior of thermoplastic polycarbonate gratings upon thermal annealing above T_g: (a) shallow patterns dewet on the substrate; (b) patterns remain stable and (c) thick patterns relax on the substrate.

When a thin polymer film is annealed at a temperature above its glass transition temperature, the polymer film gradually relaxes to a stable state, which is determined by the surface properties of the polymer and substrate and the entanglement state of the polymer. For very thin polycarbonate layer, patterns are shrunk and piled up upon annealing ascribed to strong chain entanglement interactions to get away from the substrate. When the thickness is increased, the thick top portion would fall down and reflow because of gravity. Then the pattern would be spread while maintaining the shape. A well entangled network in thin polycarbonate film results in very sluggish chain

movement to maintain structural stability. Moreover, the interfacial interactions between the polymer structure and the substrate are also believed to hinder the motion of the polymer patterns [82].

Based on the modules discussed above, the polycarbonate tube is sized with a radius of gyration R_g. According to $R_g = 0.038\sqrt{M_w}$ [83], it is 6.680 nm for polycarbonate with M_w = 30900. The relationship between the polymer dynamics and the grating thicknesses was studied in terms of the radius of gyration R_g. A series of grating heights were annealed at 250 ℃ for 30 min. The grating trench size pre- and post- annealing was collected by AFM and the normalized trench size, which is the ratio of post- over pre-annealing trench size, was calculated to characterize the wetting/dewetting behavior of the polycarbonate gratings. As illustrated in Figure 28, data points with normalized trench size larger than 1 indicated dewetting behavior of the patterns, or vice versa. For patterns with thickness ranging from 5 to 9 times of R_g, the value of normalized trench size is around 1, which implies that the polycarbonate patterns tend to stay stable upon thermal annealing. It opens up possibilities of step-and-repeat thermal nanoimprint for large scale applications. In modern lithographic techniques, the resist layer thickness has reduced to sub-50 nm along with the reduction of the critical dimension. Very thin resist layer is required due to the constraint of height-to-width aspect ratio when patterning nanostructures. When the thickness is large than 9 times of R_g, the polycarbonate gratings spread upon thermal annealing and tend to wet the substrate. It ended up with stable structures and a reduction in the gap size. One application of pattern relaxation is to determine the “end point” of polymer reflow for

high resolution patterning. Thus the unusual annealing behavior of thin polymer nanostructures has wide impact on nanolithography.

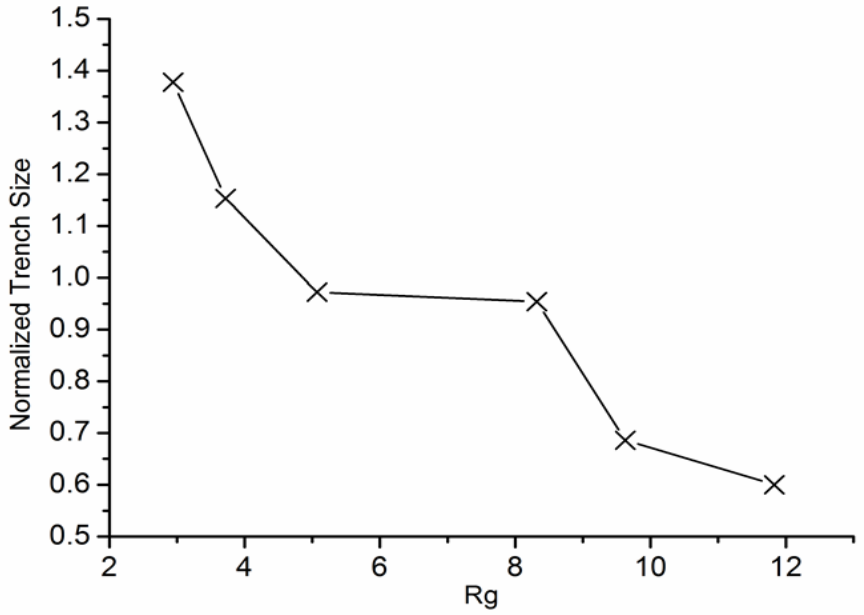

Figure 28 The plot of normalized trench size (the ratio of post- over pre-annealing grating trench size) vs pre-annealing grating height (in terms of R_g).

3.5 Polymer Reflow of Polycarbonate Gratings

As is discovered, upon thermal annealing, the polycarbonate gratings with thickness more than 9 R_g ended up with stable structures despite initial reflow, leading to a reduction in the gap size. This phenomenon can be utilized as a high resolution patterning technique, which is further studied by the following tests. The polycarbonate (M_w = 36600) was thermally imprinted on SiO_2 substrate by a SiO_2 grating mold (700

nm period, 50% duty cycle, and 250 nm depth) and the heights of the patterns were controlled to be 150 nm and 70 nm by oxygen RIE. Then the samples were annealed at 250 ℃ for 30 min to induce polymer reflow. The pattern feature sizes were characterized by JEOL JSM-7500F SEM. After thermal annealing, pattern relaxation was observed in 150 nm gratings from Figure 29(a) to (b), which showed the grating gap size shrinkage. The annealed polymer grating features were transferred into the underlying SiO_2 substrate with CHF_3 RIE process. After rinsing off the covered polymer, the transferred patterns on SiO_2 can be observed in Figure 29(c) and (d). The trench widths between the SiO_2 protrusions were reduced to 100 nm and 240 nm, with initial thickness of 150 nm and 70 nm, respectively. A smaller trench size was obtained from thicker gratings, which indicated that the trench widths after thermal annealing were related to the initial thickness of polycarbonate gratings.

The relationship between the trench widths after thermal annealing and the initial thickness of polycarbonate gratings was investigated by a serial of samples with individual grating thickness, which can be controlled by the oxygen RIE time. The trend of the trench width after annealing with the initial thickness was illustrated in Figure 30. The increasing initial thickness would result in decreasing the trench size. For the gratings with an initial thickness of 200 nm, a trench width as small as 35.0 ± 5.2 nm was achieved in Figure 29(e), which was a 90% reduction of the original feature size. This technique could be employed for high resolution patterning in nanofabrication applications.

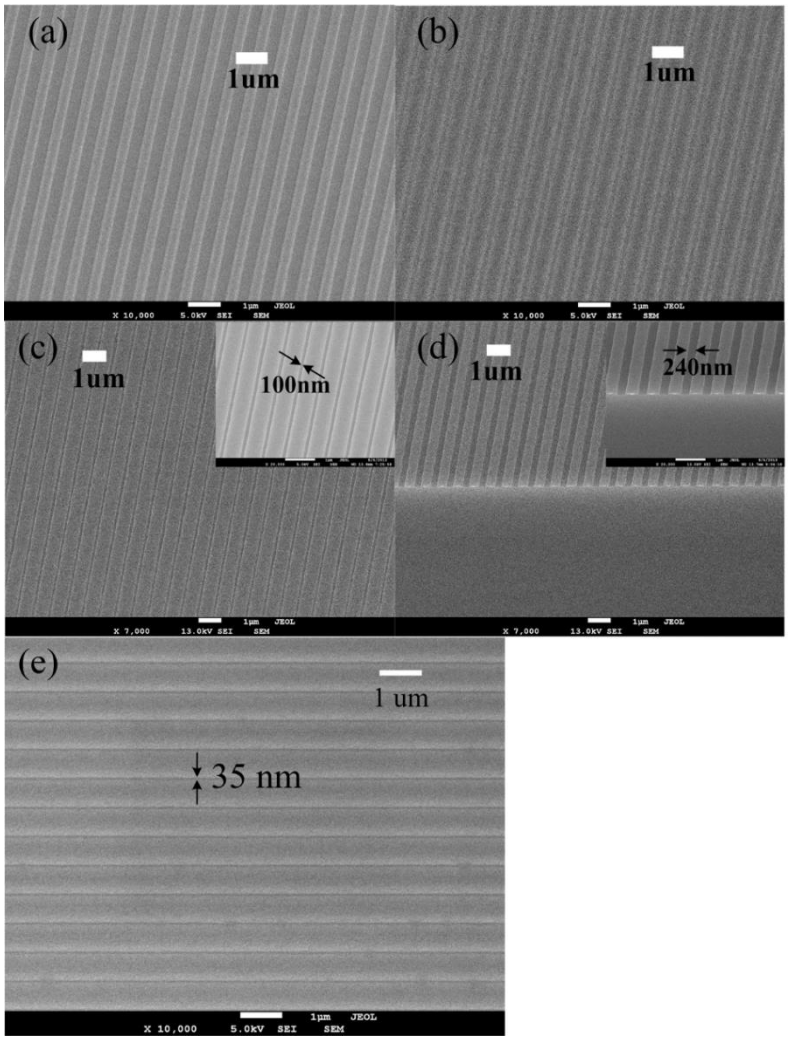

Figure 29 (a) Polycarbonate gratings (700 nm pitch, 50% duty cycle and ca.150 nm height) fabricated by thermal NIL and oxygen RIE; (b) polycarbonate gratings after thermal annealing at 250 ℃ for 30 min; (c) SiO_2 gratings by CHF_3 RIE from (b); (d) SiO_2 gratings by CHF_3 RIE from polycarbonate gratings with ca.70 nm height; and (e) 35 nm polycarbonate trenches. Inserts are at higher magnification.

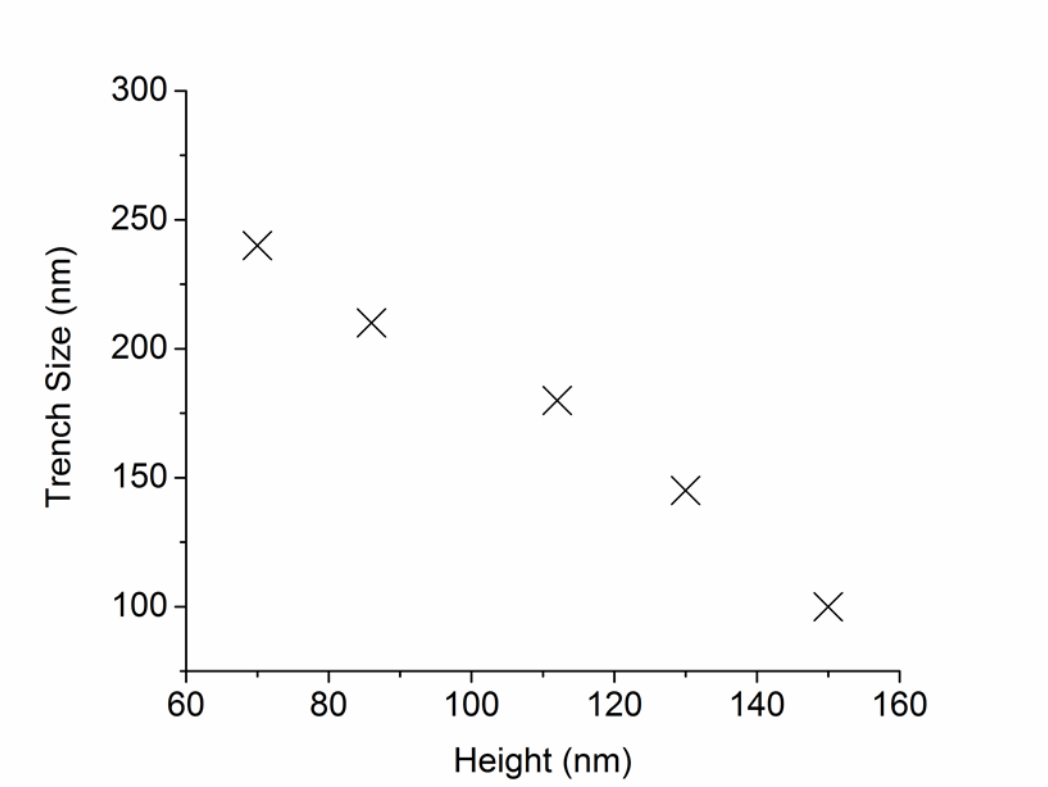

Figure 30 The plot of trench sizes after thermal annealing as a function of the initial height of the grating before thermal annealing.

3.6 Summary and Conclusion

In summary, the exceptional thermal stability of polycarbonate nanostructures on SiO_2 substrate at temperatures well above its glass transition temperature was investigated in this chapter. The phenomenon is ascribed to strong polymer chain entanglement in thin polycarbonate films, which results in very sluggish chain movement to maintain structural stability. The reflow behavior of polycarbonate gratings and the dimension information showed that three regions – dewetting, stable and spread were observed at various thicknesses. The relationship between the thermal behavior of

polycarbonate nanostructures and the initial thickness was studied in terms of R_g. The nano-structures with the height of 5 ~ 9 R_g could maintain their original morphology at temperatures well above T_g. Given the stability issue for thermoplastic polymer patterns at temperatures close to or above T_g, this technique opens up a great possibility for step-and-repeat thermal nanoimprint [84] for large scale applications with high throughput. For polycarbonate gratings above 9 R_g, it was observed that stable structures were formed despite initial reflow and the trench sizes between the gratings were reduced and determined by the initial grating thickness. In this study, trenches down to 35 nm wide were achieved by carful control of the initial thickness. This phenomenon can be utilized for high-resolution polymer patterning by determining the "end point" for polymer reflows. We have embarked on the corresponding experiments and promising results are expected in the near future.

CHAPTER IV

ANTI-STICKING EFFECTS OF POLYCARBONATE RESIDUAL LAYER IN NANOIMPRINT LITHOGRAPHY

4.1 Introduction

Nanoimprint lithography (NIL) [9, 10, 47, 85, 86] is a potential candidate for the next-generation lithography techniques for various nanostructure applications with low cost and high throughput [16, 18, 19, 22, 87]. In both thermal and UV NIL, a mold with a protruding/recessed surface pattern has a large total surface area that comes in direct contact with the imprinted polymer during imprinting. The adhesion between the polymeric material and the mold plays a key factor in this process. One of the most important problems typically encountered by NIL is the strong tendency of adhesion of the resist polymer to the mold surface during the demolding process. Adhesion effects will reduce the lifetime of the mold, degrade the quality of replication, and make the processing procedures complicated. One approach to reduce the resist polymer adhesion is to apply a thin fluorinated self-assembled monolayer (SAM) to a mold prior to imprinting as an anti-sticking layer. However, with repeated imprinting, the wearing and stability of the SAM is prone to degradation during imprinting process. This degradation requires the periodic reapplication of the SAM, which could be a critical issue for the acceptance of imprint-based technology in industrial applications.

Polycarbonate (PC) is a high performance polymer with a high glass-transition temperature (T_g = 150 ℃) and low surface free energy (34.2 mJ/m^2). Poly(methyl

methacrylate) (PMMA), a commercial thermal plastic material, has been mostly used as NIL resist. The phase behavior of a two binary PC/PMMA blend system upon heat treatment has been studied [88-90] and has shown no reactions or strong specific interactions between PC and PMMA components. In this work, we propose the application of PC as an anti-adhesive layer to a SiO_2/Si nanoimprint mold for use in PMMA NIL.

Raman spectroscopy has helped obtain molecular information in polymer materials. The Raman spectra of PC have been studied by a number of studies. In our work, we measured Raman spectra of imprinted PC under various treatments to examine PC at the molecular level. By the Raman spectroscopy study, it is possible to understand the bonding process of polymer in nanoimprint lithography and obtain information about the distribution of PC on SiO_2 surface.

4.2 Experimental

Two SiO_2 grating molds (a 600 nm period and 50% duty cycle) with 190 nm grave depth were prepared. One was coated with 1H,1H,2H,2H-perfluorodecyltrichlorosilane (FDTS) and the other has no special treatment. Polycarbonate resin with average molecular weight of 30900 was supplied by Scientific Polymer Product Inc. 3 wt% polycarbonate solution were prepared by dissolving polycarbonate powders into cyclopentanone solvent. Polycarbonate thin film was obtained by spin-coating the prepared solution on SiO_2 substrate, followed by solvent removal on a hotplate for 3 min at 90 ℃. Both molds were carried out the imprinting

process on PC thin film at 220 ℃ under a pressure of 5 MPa for 5 min. Raman spectra in the range of 1050-3200 cm^{-1} were measured on a DPSS laser (Laser Quantum) excited Raman spectrometer (Horiba LabRAM HR Evolution) with a spectral resolution of 0.65 cm^{-1}. The continuous source emits at 512 nm and has a power of about 25 mW. The beam was passed along the axis of a 5 um diameter rod. We measured the water contact angle of the mold surface using a commercially available contact angle meter (VCA Optima, AST Products, INC.). 800-um-thick PMMA sheets purchased From Mitsubishi Rayon Co., Ltd. were used for nanoimprinting. The pattern was measured by using atomic force microscope (Bruker Dimension Edge AFM).

4.3 Results and Discussion

4.3.1. PC imprinted by the FDTS treated mold

Figure 31(a) shows the atomic force microscopy (AFM) of PC imprinted by the FDTS treated mold. The imprinted PC pattern is etched by inductively coupled plasma (ICP) for residual layer removal, as shown in Figure 31(b). Then the etched sample is rinsed off with cyclopentanone for 10 min. Figure 31(c) shows that 6.4 ± 0.7 nm thick PC gratings remained and adhered to the substrate after the rinse. It is exhibited polymer bonding to the SiO_2 substrate during thermal imprinting. Therefore, for PC imprinted with the bare SiO_2 mold, a thin layer of PC should be applied to the mold surface.

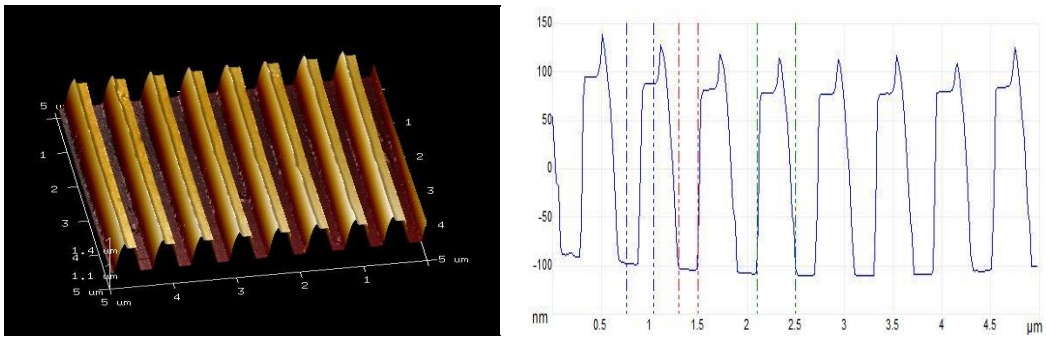

(a)

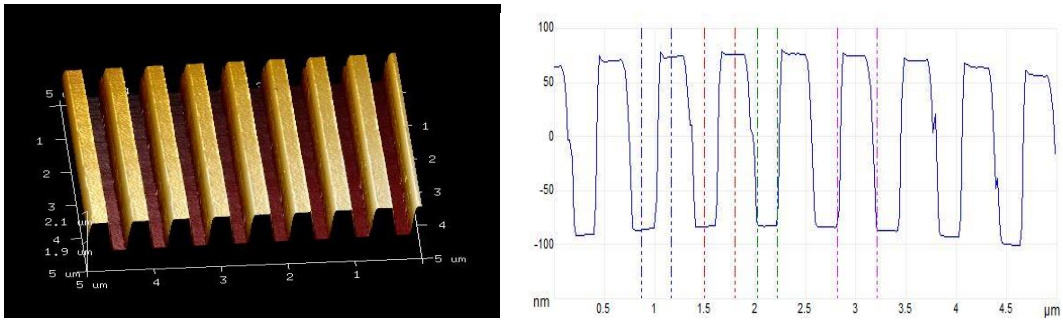

(b)

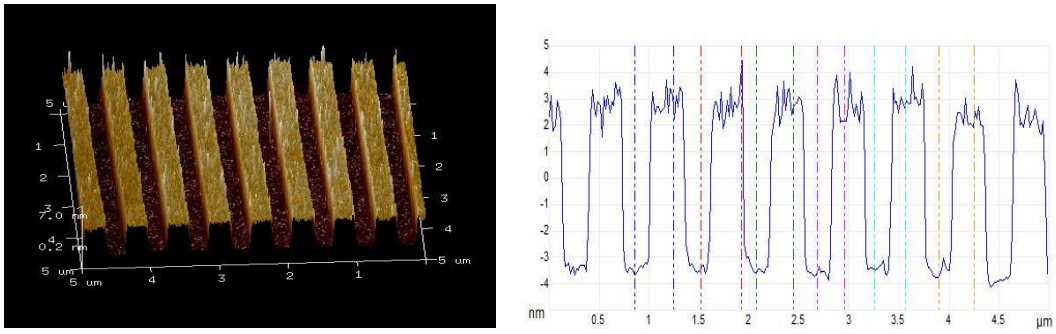

(c)

Figure 31 AFM images of imprinted PC patterns: (a) NIL at 220 ℃ and 5 MPa; (b) NIL and 35 s ICP treatment; (c) rinse off ICP treated gratings with cyclopentanone-acetone-IPA for 10 min.

4.3.2. Raman spectroscopy

The Raman spectrum of PC thin film is recorded and shown in Figure 32. Our measurement of 200 nm PC thin film is, in general, in excellent agreement with previous studies [91-93]. There are intense bands due to C-H stretching in the region near 3000 cm^{-1}. The C=O stretching mode of PC appears at 1774 cm^{-1} and phenyl ring vibration mode appears at 1630 cm^{-1}. The spectrum shows a considerable number of largely overlapped bands in the range below 1600 cm^{-1}, which are associated with stretching of the O-C-O group.

The Raman spectrum of PC treated with: 1) NIL on SiO_2 substrate, 2) NIL and ICP on SiO_2 substrate, 3) NIL on the bare SiO_2 mold were recorded after all samples were rinsed off with cyclopentanone. Figure 32 shows that for all treatments there are overlapping Raman modes in the region near 3000 cm^{-1}, which demonstrates a PC residual layer is remained and bonded to SiO_2 surface during thermal imprinting and it could not be removed with the rinse. It is also shown that PC bonding occurs on the bare SiO_2 mold surface with imprint, which refers to coverage of PC residual layer on the mold surface after NIL.

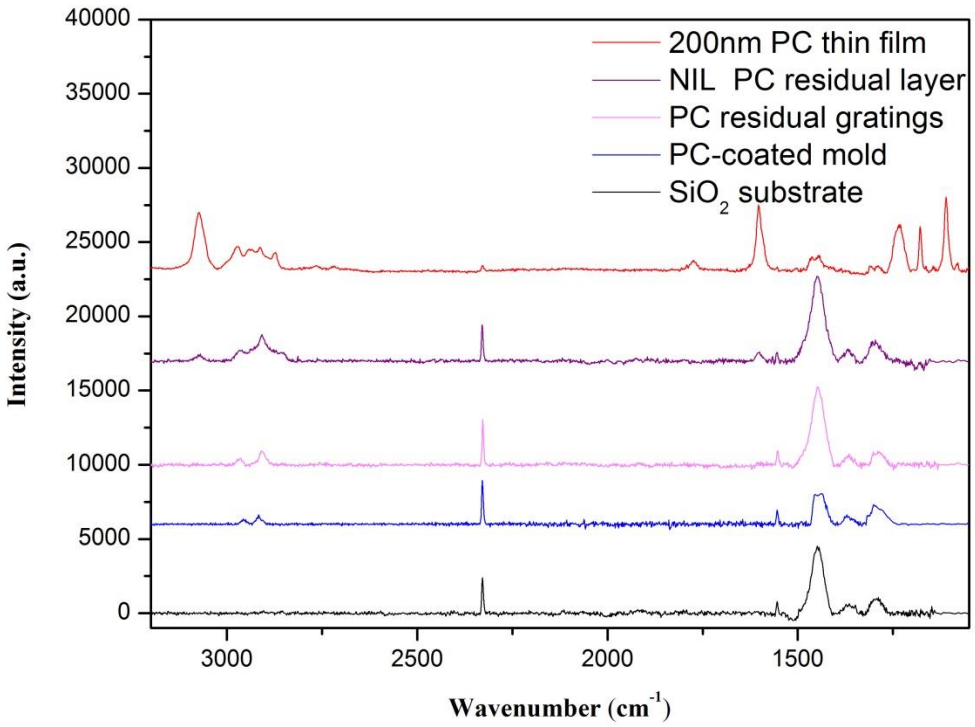

Figure 32 The Raman spectrum of SiO_2 substrate and PC under various conditions.

4.3.3. Contact angle

Figure 33(a) and (b) show the measured water contact angles of the blank and PC-coated mold surfaces, respectively. The water contact angle for blank mold is 39 ° while the markedly increased value of water contact angle for the PC-coated mold is up to 118.5 ° or 79.5 ° higher than that of the blank mold. This result indicates that the hydrophobic property of the mold surface is enhanced by the addition of polycarbonate.

Therefore, a PC thin film provides a sufficient contact angle for use as an anti-sticking layer on the mold.

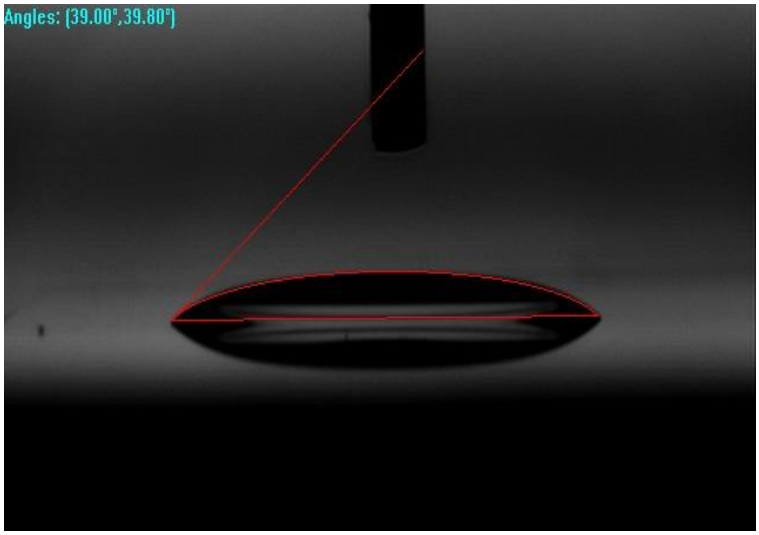

(a)

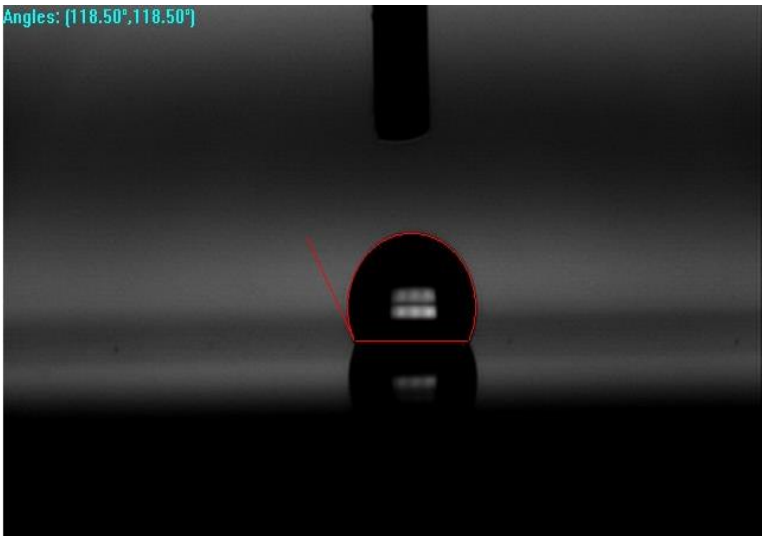

(b)

Figure 33 Photos of water droplets on (a) the blank mold surface; (b) the PC-coated mold surface.

4.3.4. PMMA sheet NIL

The mold coated with PC was used to imprint PMMA sheets at 120 ℃ and 5 MPa. Imprinting was repeated for more than 10 times. Figure 34(a) shows the AFM image of imprinted PMMA patterns after imprinting 10 times, whereas Figure 34(b) shows the overall image of the imprinted area. The PMMA gratings were successfully obtained with a great yield up to 100%. These results show the great potential and imprint durability of PC as an anti-sticking layer for thermal-NIL.

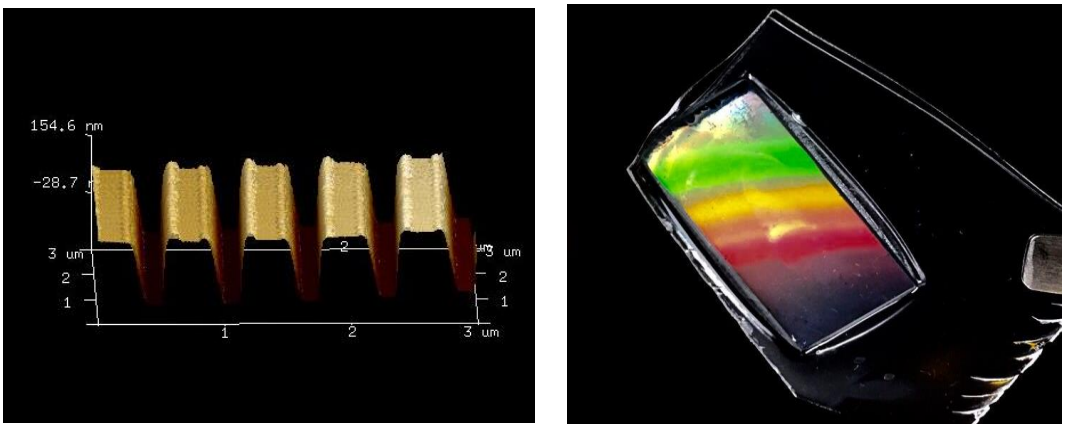

(a) (b)

Figure 34 (a) The AFM image of PMMA patterns imprinted by the PC-treated mold after imprinting 10 times; (b) an overall image of the imprinted PMMA sheet.

4.4 Summary and Conclusion

The PC thin film is suitable for the anti-sticking application of hot embossing nanoimprint lithography because of its high glass-transition temperature and good

durability. We demonstrated a thin layer of the PC film is deposited on SiO_2/Si nanoimprint molds by NIL as an anti-sticking layer. PMMA thermal imprinting was achieved using the PC-coated mold. Furthermore, PC is a good UV-transparent material and is also expected to be suitable for deposition on UV-NIL molds made of transparent materials. The durability measurement will be conducted for future study.

CHAPTER V

VOLUME-EXPANSION POLYMERIZATION FOR UV-CURABLE NANOIMPRINT

5.1 Introduction

Nanoimprint lithography (NIL) has been regarded as one of the next-generation lithography techniques due to its ability to fabricate nanoscale structures with low cost and high throughput. Although both thermal [9-11] and UV [26, 94, 95] NIL have demonstrated sub-10 nm resolution, the adoption of NIL by industry has been very limited. The main reason is that the density of pattern defects cannot satisfy the stringent requirement of commercial lithographic technique.

The origin of pattern defects in nanoimprint can be linked to multiple factors. Some factors, such as dust particles and non-uniform imprint pressure, can be managed by better tooling or careful processing. However, the interaction forces at the mold/resist and resist /substrate interfaces are not easily controlled and they often contribute to defect generation during the demolding stage of NIL.

UV-curing NIL is favored in microelectronic fabrication because its processing conditions are similar to optical lithography. However, the resist volume shrinkage after curing in UV NIL not only affects the pattern fidelity [86, 96-100] but also induces pattern defects in mold releasing step. Park et. al. [101] has experimentally demonstrated that both adhesion and friction force between mold and resist contribute to the total demolding force. When volume shrinkage occurs, the friction force increases

dramatically while the adhesion force remains nearly constant. The increase of friction force is due to the large residual stress exerted on mold sidewalls by the resist. Conventional techniques to lower demolding forces such as mold anti-adhesion coating and resist additive only address the adhesion part and have small effect on the friction force. Thus their effectiveness is limited and the demolding step is still a significant cause for defect generation.

Since friction force is directly proportional to resist shrinkage, it may be conducive to reduce or even completely eliminate volume shrinkage in UV NIL. When UV-curable monomers polymerizes, the van der Waals interactions among monomer molecules are converted into covalent bonds. The van der Waals interaction range is around 3-5 Å while typical covalent bond lengths are 1-2 Å, thus volume shrinkage is unavoidable in traditional UV-curing resist formulations. Acrylate-based UV resists have a volume shrinkage in the range of 5% to 20%, while epoxy-based UV resists have a volume shrinkage in the range of 3% to 10%.

Many methods have been employed to reduce the shrinkage, including inorganic additives, choosing monomers with low concentration of functional groups, and using bulky monomer molecules [53, 102-104]. Although they have some effectiveness in lowering volume shrinkage, these methods cannot completely remove shrinkage and the lower concentration of reactive groups often results in lower cohesive strength of the cured resist.

In this work, we address the shrinkage issue in UV NIL by utilizing volume-expansion polymerization. Spiroorthocarbonate is found to be able to undergo double

ring opening polymerization when catalyzed by photo acid at room temperature [105-109]. The double ring opening process converts two covalent bonds into van der Waals interactions, which results in volume expansion. By mixing the spiroorthocarbonate monmer with an epoxy monomer, it is possible to adjust the volume shrinkage of the cured resist. We show that new UV NIL resist formulations containing various amounts of spiroorthocarbonate monomers can achieve zero volume change or even volume expansion after curing. The use of volume-expansion polymerization in UV NIL presents a capability to tune volume change in UV resist. It opens up a new route towards managing residual stress in cured structures, hence solving pattern fidelity and demolding force.

5.2 Experimental

5.2.1. Synthesis and characterization of spiro-orthocarbonate

In this study, 1,5,7,11-tetraoxaspiro[5,5] undecane (shown in Figure 35) has been introduced to the resist formula to compensate the volume shrinkage caused by the curing of commonly used epoxy compound. 1,5,7,11-tetraoxaspiro[5,5] undecane was synthesized through the reaction of tetramethyl orthocarbonate with 1,3-Propanediol [110], and the reaction profile is shown in Figure 35. Tetramethyl orthocarbonate (1.36 g, 10 mmol) and ethylene glycol (1.24 g, 20.0 mmol) in dry xylene (33 mL) was added anhydrous p-toluenesulfonic acid (57 mg, 0.03 mmol) to form a heterogeneous mixture. The mixture was heated at a bath temperature of 110℃ for 9 h. During the reaction

methanol was distilled. The resulting product was cooled to room temperature, and then added a few drop of trimethylamine. The mixture was washed with aqueous $NaHC0_3$ and extracted with ether. The organic layer was dried through anhydrous $MgSO_4$ and then evaporated. After recrystallized from methanol, the residual solid material was obtained.

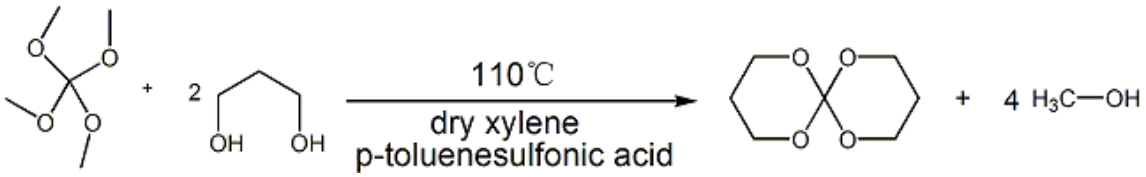

Figure 35 Reaction profile of synthesizing 1,5,7,11-tetraoxaspiro[5, 5] undeane.

The synthesized product was characterized by ^{1}H-NMR spectrum, which is shown in Figure 36. In the ^{1}H-NMR spectrum, two peaks at 1.805 ppm and 4.059 ppm are attributed to the methylenes protons (CH_2) and the methylenes protons adjacent to the ether oxygens (CH_2O), and the area of the former peak is two times of the latter one's, which is consistent with the structure of 1,5,7,11-tetraoxaspiro[5,5] undecane. The ^{1}HNMR data demonstrate the desired 1,5,7,11-tetraoxaspiro[5,5] undecane is obtained.

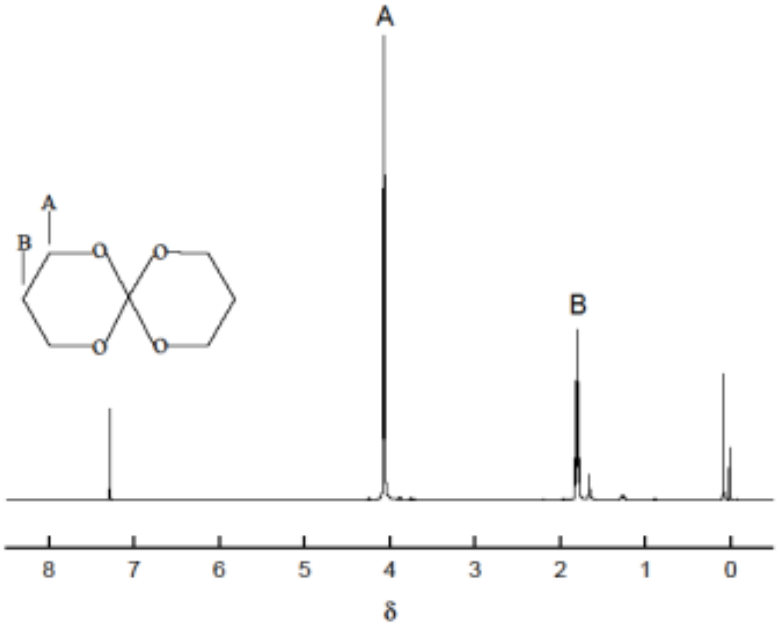

Figure 36 [1]HNMR spectrum of the synthesized product.

5.2.2. Resist formulation and nanoimprint

A SiO_2 grating mold (a 20 um period, 5 um protrusion, and 15 um grave) is used in this study. The grating was fabricated on fused silica by lithography and reactive-ion etching with 300 nm grave depth. The mold surface was coated with 1H,1H,2H,2H-perfluorodecyltrichlorosilane for anti-sticking and easy mold releasing [111]. The nanoimprint resist is composed of an epoxy monomer (a representative structure is shown in Figure 37(a)), a spiro-orthocarbonate monomer (see Figure 35), and a photoacid generator (PAG) (Figure 37(b)). The mixtures of various spiro-orthocarbonate: epoxy compositions were prepared and all formulations have 5% photoacid generator.

Organic solvents, such as propylene glycol monomethyl ether acetate (PGMEA), could be used to dissolve spiro-orthocarbonate and adjust the viscosity of the resist so that a thin film could be obtained.

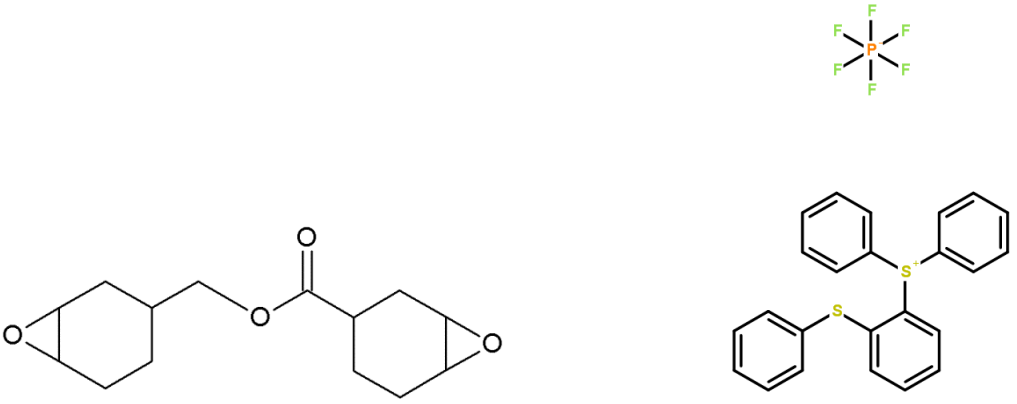

(a) (b)

Figure 37 Representative structures of resist materials. (a) Epoxy monomer; (b) Photoacid generator.

The liquid resist was dripped on silicon oxide substrate, followed by solvent removal on a hotplate for 3 min at 90 ℃. The imprinting process was carried out at room temperature and a pressure of less than 0.1 MPa. The wavelength used for UV curing was 365 nm and the exposure dose was 7.1 mW/cm^2.

5.2.3. Characterization of imprinted structures

Volume change is usually observed in UV-cured materials. To elevate the amount of the volume change, the pattern dimension was measured by using atomic

force microscope (Bruker Dimension Edge AFM). The structural information of the resist gratings patterned by nanoimprint was also investigated. Optical birefringence in gratings was directly visualized in a polarizing microscope with crossed-polarizers (Nikon Eclipse LV100POL).

5.3 Results and Discussion

5.3.1. Spiro-orthocarbonate in UV-curable resist

The composed UV-curable resists with and without spiro-orthocarbonate were used to pattern desired structure with NIL. Figure 38(a) shows a pattern of pure epoxy, while Figure 38(b) shows a pattern of spiro-orthocarbonate: epoxy = 1: 2, after imprinting and curing. These results demonstrate that micro-scale patterns can be easily achieved with the composed resists. For pure epoxy resist without spiro-orthocarbonate, gratings contraction and distortion were observed because of volume shrinkage; for the resist with spiro-orthocarbonate, an obvious protrusion was seen at each edge of gratings. These protrusions demonstrate volume expansion by adding spiro-orthocarbonate in UV resist after curing.

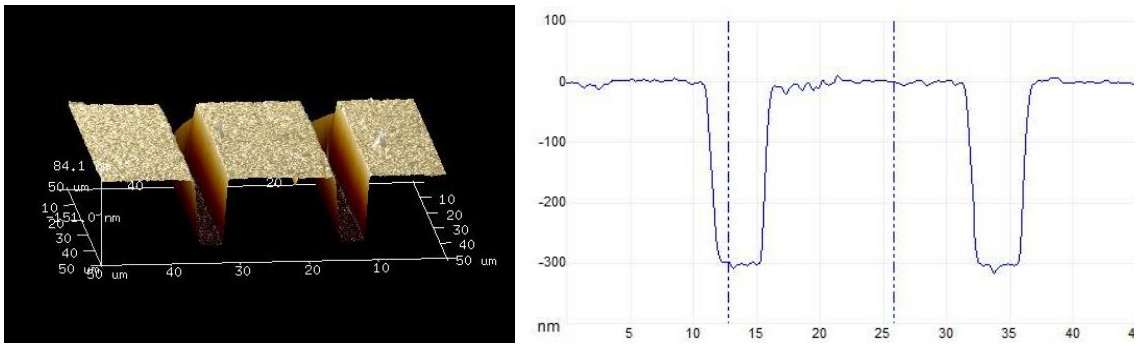

(a)

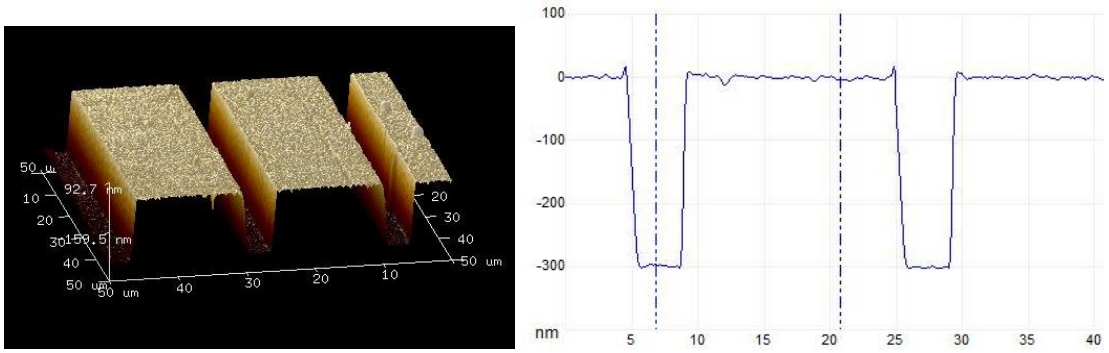

(b)

Figure 38 AFM images of imprinted and UV-cured resist patterns: (a) pure epoxy; (b) spiro-orthocarbonate: epoxy = 1: 2.

5.3.2. Volume-expansion in UV nanoimprint

Figure 39 shows cross sections of the mold used for imprinting and imprinted samples. The amount of volume change was determined by comparing pattern dimensions after curing with the mold cavity width. The bottom of the mold cavity and the top portion of resist were measured by atomic force microscope (AFM).

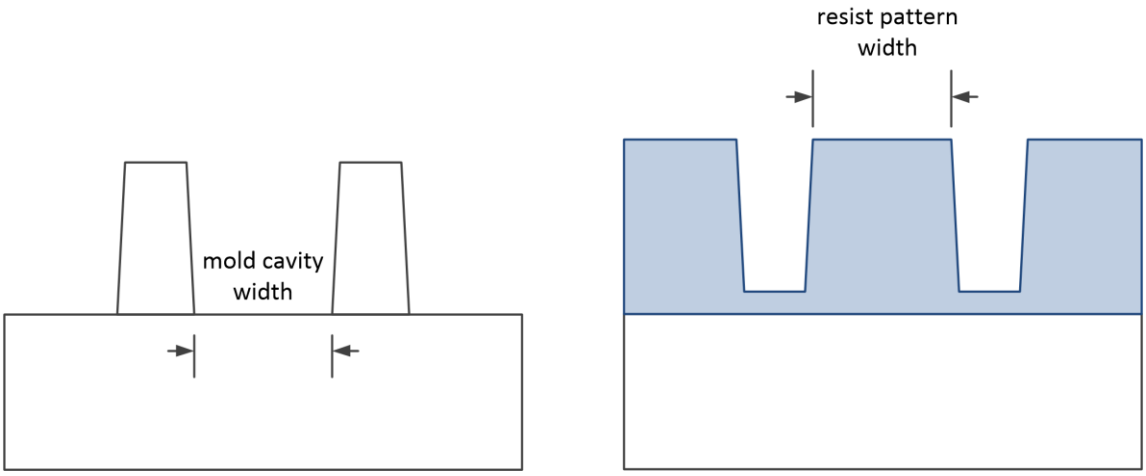

Figure 39 Cross sections of mold and resist pattern.

Table 1 Volume changes of various compositions.

	Mold (μm)	**Epoxy only (μm)**	**Spirocarbonate : epoxy 1:9 (μm)**	**Spirocarbonate : epoxy 1:2 (μm)**
Size	15.021±0.066	14.765±0.055	15.011±0.048	15.599±0.048
Vol change		-1.70%	-0.07%	+3.85%

Table 1 shows the volume changes of various compositions. After curing, polymerizations of pure epoxy monomers proceed along with ~1.7% of volume shrinkage. Before a polymerization, there are van der Waals interactions among monomers and monomers exist apart from each other in a van der Waals distance (VDWD) ranging from 3 to 5 Å. After the polymerization, the van der Waals interactions are converted to covalent bonds that are usually smaller than the VDWD

with a length of 1-2 Å [112]. As a consequence, volume shrinkage is unavoidable mainly from proximity of monomer molecules caused by the polymerization. Reactions of spiro-orthocarbonate: epoxy = 1: 2 indicate a relatively high expansion in volume (~3.85%). A double ring-opening polymerization of spiro-orthocarbonate causes a conversion of two covalent bonds to van der Waals interactions (Figure 40), resulting in offset of volume shrinkage or even volume expansion [112]. The ratio of spiro-orthocarbonate to epoxy is optimized to 1 to 9 with a volume change of ~0.07%, which is approximate zero volume shrinkage.

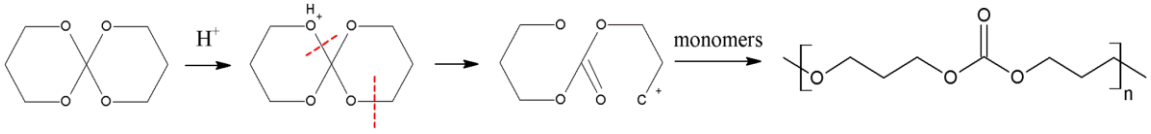

Figure 40 Spiro-orthocarbonate double ring opening polymerization.

5.3.3. Residual stress in imprinted structures

Volume shrinkage in a UV curable resist by polymerization induces residual stress and makes it difficult to release mold [86, 97, 100, 101]. According to Stress-Optical law, the magnitude of the refractive index at each point in the material is directly related to the stress state at that point. Upon the application of residual stress in the grating lines, the imprinted material exhibits the property of optical birefringence. Visualization and quantitative measurement of residual stress is possible through optical birefringence measurement in polarizing microscope with crossed polarizers.

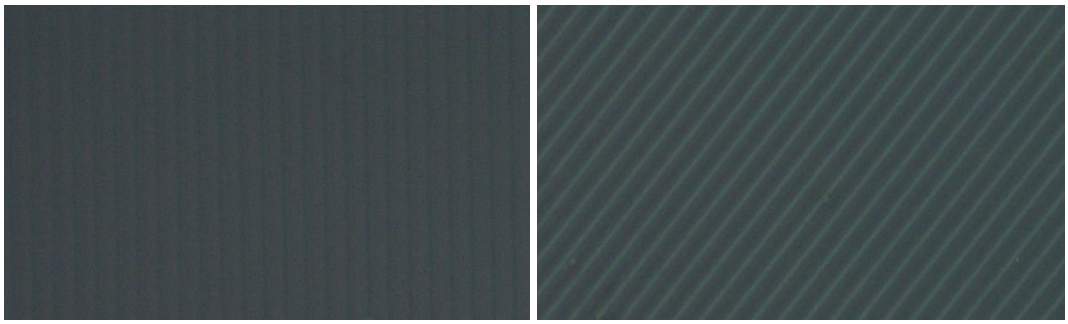

(a)

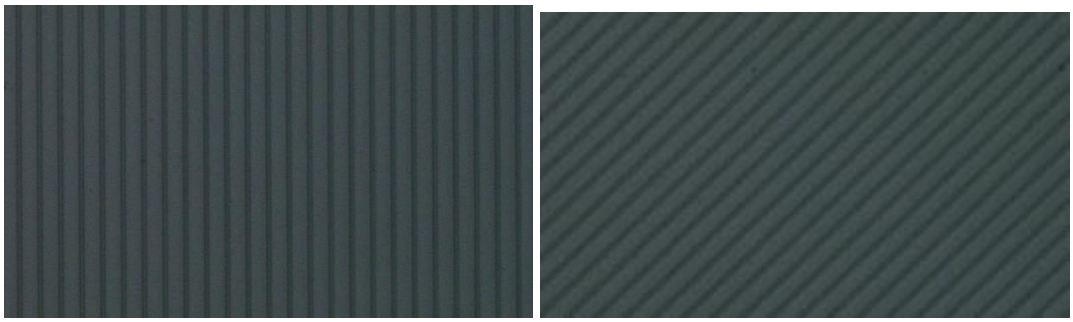

(b)

Figure 41 Polarizing microscope images of cured UV-resist gratings: (a) pure epoxy; (b) spiro-orthocarbonate: epoxy = 1: 9.

The polarizing microscope images of UV-resist gratings are shown in Figure 41. In pure epoxy gratings (Figure 41(a)), dark images were observed when the grating line was parallel. If the incident light was polarized parallel to the gratings, the polarization state of the incident light would be unaffected and the polarized light would be completely blocked by the top crossed polarizer, leading to a dark image of the sample. When the gratings were rotated at 45 °, image emerged brighter at grating edges. This observation clearly demonstrates the optical birefringence due to residual stress in pure

epoxy gratings. The birefringence would cause an optical retardation and therefore rotate the polarization direction of the incident light and develop a net component along the polarization direction of the top polarizer, leading to a bright image of the sample. In Figure 41(b), no optical birefringence was exhibited in the mixture of spiro-orthocarbonate: epoxy = 1: 9 patterns. Optical isotropy indicates there is no residual stress observed, which refers to zero volume shrinkage. These phenomena consist with the results we have measured before.

5.4 Summary and Conclusion

In summary, we have developed a new UV-curable resist based on cationic copolymerization of spiro-orthocarbonate and epoxy monomers. The liquid resist can be imprinted micro-scale patterns easily. The double ring-opening reaction during the polymerization overcomes volume shrinkage. With the composition optimization, zero volume shrinkage is achieved, which facilitates separation of the mold from the substrate after imprinting and increases the fidelity of the imprinted patterns. Nanoscale patterns and friction force measurement will be developed for further study.

CHAPTER VI

SUMMARY

Nanoimprint lithography (NIL) is envisioned as the most promising candidate for the next-generation lithography due to its high resolution and throughput at a low cost. It is an inherently simple lithographic technique in which a hard mold with designed patterns is pressed directly into an organic resist spin-coated on a substrate. The patterns are solidified with applications of heat and pressure or shining of UV light and formed on the resist after releasing the mold. Both thermal and UV nanoimprint have demonstrated sub-10 nm resolution. Nowadays, NIL has been widely used in various applications, such as organic electronics, optoelectronics, and microfluidics. Although NIL has attracted much attention in the micro- and nano-fabrication fields, the adoption of nanoimprint in industry has been very limited and both conventional thermal and UV NIL have several limitations.

Conventional thermal NIL commonly imprints thermal-plastic polymers upon heating to 70–80 ℃ above the T_g of the used materials for a significant reduction in the resists' viscosities. A long process cycle time is necessary in thermal NIL for the heating up and cooling down stages and hence leads to a limitation in the throughput of the NIL process. In addition, high imprinting temperature puts greater demands on the equipment setup and therefore increases the cost. Moreover, multiple patterning cannot be implemented within the same substrate because subsequent imprint requires a high

temperature above the T_g, which will inevitably destroy the patterns formed in preceding imprint. Therefore large scale application is limited in thermal NIL.

UV NIL is usually imprinted at room temperature because the lower viscosity of UV curable resists easily ensures full filling of the features of the mold. However, a big challenge in UV NIL is a high rate of defect generation attributed to resist volume shrinkage and the demolding process.

In this study, we concentrated on developing methods and material beyond conventional nanoimprint lithography and proposed new schemes to overcome the limitations of conventional NIL by utilizing three factors: mold, the interface between mold and resist, and resist.

A new synergistic thermal and UV nanoimprint lithography (STUV-NIL) mold was fabricated by integrating a transparent mold with a transparent heater. This design enabled the imprinted resist to be cured by thermal energy and UV light spontaneously, which may lead to less defects and higher throughput.

The exceptional thermal stability of polycarbonate nanostructures fabricated by thermal NIL has been investigated, which can be ascribed to chain entanglement in polymer thin film. We experimentally characterized the reflow behavior of polycarbonate nanostructures with various initial thicknesses in terms of R_g; three regions – dewetting, stability and relaxation – were observed with increasing pattern thickness. One application of pattern relaxation is to determine the “end point” of polymer reflow for high resolution patterning. In this work, a minimum trench size of ca.

35 nm was achieved with starting patterns of 700 nm pitch (50% duty cycle) gratings. This phenomenon could have wide impact on nanolithography.

Polycarbonate (PC) has also been applied as an anti-sticking layer on nanoimprint molds, replacing the self-assembled monolayer currently used. A SiO_2/Si mold was successfully coated with a PC thin layer by thermal imprinting. The hydrophobic property of the mold surface was enhanced by the addition of polycarbonate. Therefore, the PC thin film provides a sufficient contact angle for its use as an anti-sticking layer in NIL. PMMA resist gratings were successfully obtained by thermal NIL using the PC-coated mold with a great yield up to 100%. The PMMA patterns were maintained after repeating the imprinting for more than 10 times. It shows great potential and imprint durability of PC as an anti-sticking layer for thermal-NIL.

For UV NIL, polymerizations are usually accompanied by volume shrinkage, which causes serious problems in the field of UV nanoimprinting, such as residual stress, demolding problems and defects. Thus, it is requisite to depress and overcome the volume shrinkage during polymerizations in UV nanoimprint. Epoxy-based UV resists have a volume shrinkage in the range of 3% to 10%. "Expanding monomer", which shows volume expansion during polymerization, has been conceptualized. Spiro-monomer-bearing, compactly folded, labile bicyclic bonds such as spiro-orthocarbonate has been used as one of the candidates in this study. Spiro-orthocarbonate is a monomer that undergoes volume expansion upon cationic ring-opening polymerization. By mixing the spiro-orthocarbonate monomer with an epoxy monomer, it is possible to adjust the volume shrinkage of the cured resist or achieve zero volume change after curing. With

zero volume change, there will be no residual stress left in the cured resist structures. It is also expected that zero volume change of resist after curing will lower the separation energy required during demolding. Thus the nanoimprint pattern defects caused by residual stress and high demolding energy are expected to be reduced.

REFERENCES

[1] S. D. Berger and J. M. Gibson, "New approach to projection-electron lithography with demonstrated 0.1 μm linewidth," *Applied Physics Letters*, vol. 57, p. 153, 1990.

[2] K. Wilder, C. F. Quate, B. Singh, and D. F. Kyser, "Electron beam and scanning probe lithography: A comparison," *Journal of Vacuum Science & Technology B: Microelectronics and Nanometer Structures*, vol. 16, p. 3864, 1998.

[3] H. I. Smith and D. C. Flanders, "X-ray lithography — A review and assessment of future applications," *Journal of Vacuum Science and Technology*, vol. 17, p. 533, 1980.

[4] D. L. Windt, "Multilayer facilities required for extreme-ultraviolet lithography," *Journal of Vacuum Science & Technology B: Microelectronics and Nanometer Structures*, vol. 12, p. 3826, 1994.

[5] C. W. Gwyn, R. Stulen, D. Sweeney, and D. Attwood, "Extreme ultraviolet lithography," *Journal of Vacuum Science & Technology B: Microelectronics and Nanometer Structures*, vol. 16, p. 3142, 1998.

[6] R. H. Stulen, "13-nm extreme ultraviolet lithography," *IEEE Journal of Selected Topics in Quantum Electronics*, vol. 1, p. 970, 1995.

[7] C. J. Hawker and T. P. Russell, "Block copolymer lithography: merging “bottom-up” with “top-down” processes," *MRS Bulletin*, vol. 30, p. 952, 2011.

[8] M. P. Stoykovich, H. Kang, K. C. Daoulas, G. Liu, C.-C. Liu, J. J. d. Pablo, *et al.*, "Directed self-assembly of block copolymers for nanolithography fabrication of

isolated features and essential integrated circuit geometries," *ACS Nano,* vol. 1, p. 168, 2007.

[9] S. Y. Chou, P. R. Krauss, and P. J. Renstrom, "Imprint of sub-25 nm vias and trenches in polymers," *Applied Physics Letters,* vol. 67, p. 3114, 1995.

[10] S. Y. Chou, P. R. Krauss, and P. J. Renstrom, "Imprint lithography with 25-nanometer resolution," *Science,* vol. 272, p. 85, 1996.

[11] S. Y. Chou, P. R. Krauss, W. Zhang, L. Guo, and L. Zhuang, "Sub-10 nm imprint lithography and applications," *Journal of Vacuum Science & Technology B: Microelectronics and Nanometer Structures,* vol. 15, p. 2897, 1997.

[12] M. Li, L. Chen, and S. Y. Chou, "Direct three-dimensional patterning using nanoimprint lithography," *Applied Physics Letters,* vol. 78, p. 3322, 2001.

[13] W. Zhang and S. Y. Chou, "Multilevel nanoimprint lithography with submicron alignment over 4 in. Si wafers," *Applied Physics Letters,* vol. 79, p. 845, 2001.

[14] I. Martinia, M. Kampa, F. Fischera, L. Worschecha, J. Koethb, and A. Forchela, "Fabrication of quantum point contacts and quantum dots by imprint lithography," *Microelectronic Engineering,* vol. 57–58, p. 397, 2001.

[15] I. Martini, J. Dechow, M. Kamp, A. Forchel, and J. Koeth, "GaAs field effect transistors fabricated by imprint lithography," *Microelectronic Engineering,* vol. 60, p. 451, 2002.

[16] L. Guo, P. R. Krauss, and S. Y. Chou, "Nanoscale silicon field effect transistors fabricated using imprint lithography," *Applied Physics Letters,* vol. 71, p. 1881, 1997.

[17] C. C. Ceden, J. Seekampa, A. P. Kama, T. Hoffmanna, S. Zankovycha, C. M. S. Torres, *et al.*, "Nanoimprint lithography for organic electronics " *Microelectronic Engineering,* vol. 61-62, p. 25, 2002.

[18] M. Li, J. Wang, L. Zhuang, and S. Y. Chou, "Fabrication of circular optical structures with a 20 nm minimum feature size using nanoimprint lithography," *Applied Physics Letters,* vol. 76, p. 673, 2000.

[19] P. R. Krauss and S. Y. Chou, "Nano-compact disks with 400 Gbit/in 2 storage density fabricated using nanoimprint lithography and read with proximal probe," *Applied Physics Letters,* vol. 71, p. 3174, 1997.

[20] M. Austin and S. Y. Chou, "Fabrication of nanocontacts for molecular devices using nanoimprint lithography," *Journal of Vacuum Science & Technology B: Microelectronics and Nanometer Structures,* vol. 20, p. 665, 2002.

[21] J. Moritz, S. Landis, J. C. Toussaint, P. Bayle-Guillemaud, B. Rodmacq, G. Casali, *et al.*, "Patterned media made from pre-etched wafers: A promising route toward ultrahigh-density magnetic recording," *IEEE Transactions on Magnetics,* vol. 38, p. 1731, 2002.

[22] H. Cao, Z. Yu, J. Wang, J. O. Tegenfeldt, R. H. Austin, E. Chen, *et al.*, "Fabrication of 10 nm enclosed nanofluidic channels," *Applied Physics Letters,* vol. 81, p. 174, 2002.

[23] P. M. Moran and C. Robert, "Microstamping of freestanding bipolymer features," *Applied Physics Letters,* vol. 78, p. 3741, 2001.

[24] A. Pepin, P. Youinou, V. Studer, A. Lebib, and Y. Chen, "Nanoimprint lithography for the fabrication of DNA electrophoresis chips," *Microelectronic Engineering,* vol. 61-62, p. 927, 2002.

[25] V. Studer, A. Pepin, Y. Chen, and A. Ajdari, "Fabrication of microfluidic devices for AC electrokinetic fluid pumping," *Microelectronic Engineering,* vol. 61-62, p. 915, 2002.

[26] M. Colburn, S. Johnson, M. Stewart, S. Damle, T. Bailey, B. Choi, *et al.,* "Step and flash imprint lithography: A new approach to high-resolution patterning," *SPIE Proceedings,* vol. 3676, p. 379, 1999.

[27] R. S. Mackay, I. McMackin, J. Choi, P. Schumaker, V. Nguyen, F. Xu, *et al.,* "Step and Repeat UV nanoimprint lithography tools and processes," *SPIE Proceedings,* vol. 5374, p. 222, 2004.

[28] H. Schift, "Nanoimprint lithography: An old story in modern times? A review," *Journal of Vacuum Science & Technology B: Microelectronics and Nanometer Structures,* vol. 26, p. 458, 2008.

[29] L. J. Guo, "Nanoimprint lithography: Methods and material requirements," *Advanced Materials,* vol. 19, p. 495, 2007.

[30] J. Taniguchi, Y. Tokano, I. Miyamoto, M. Komuro, and H. Hiroshima, "Diamond nanoimprint lithography," *Nanotechnology,* vol. 13, p. 592, 2002.

[31] L. Tao, S. Ramachandran, C. T. Nelson, M. Lin, L. J. Overzet, M. Goeckner, *et al.,* "Durable diamond-like carbon templates for UV nanoimprint lithography," *Nanotechnology,* vol. 19, p. 105302, Mar 12 2008.

[32] S. W. Pang, T. Tamamura, M. Nakao, A. Ozawa, and H. Masuda, "Direct nano-printing on Al substrate using a SiC mold," *Journal of Vacuum Science & Technology B: Microelectronics and Nanometer Structures,* vol. 16, p. 1145, 1998.

[33] N. Koo, M. Bender, U. Plachetka, A. Fuchs, T. Wahlbrink, J. Bolten, *et al.*, "Improved mold fabrication for the definition of high quality nanopatterns by Soft UV-Nanoimprint lithography using diluted PDMS material," *Microelectronic Engineering,* vol. 84, p. 904, 2007.

[34] K. Pfeiffer, M. Fink, G. Ahrens, G. Gruetzner, F. Reuther, J. Seekamp, *et al.*, "Polymer stamps for nanoimprinting," *Microelectronic Engineering,* vol. 61-62, p. 393, 2002.

[35] N. Roos, H. Schulz, L. Bendfeldt, M. Fink, K. Pfeiffer, and H.-C. Scheer, "First and second generation purely thermoset stamps for hot embossing," *Microelectronic Engineering,* vol. 61-62, p. 399, 2002.

[36] F. Hua, Y. Sun, A. Gaur, M. A. Meitl, L. Bilhaut, L. Rotkina, *et al.*, "Polymer imprint lithography with molecular-scale resolution," *Nano Letters,* vol. 4, p. 2467, 2004.

[37] A. Amirsadeghi, J. J. Lee, and S. Park, "Surface adhesion and demolding force dependence on resist composition in ultraviolet nanoimprint lithography," *Applied Surface Science,* vol. 258, p. 1272, 2011.

[38] F. A. Houle, C. T. Rettner, D. C. Miller, and R. Sooriyakumaran, "Antiadhesion considerations for UV nanoimprint lithography," *Applied Physics Letters,* vol. 90, p. 213103, 2007.

[39] F. A. Houle, E. Guyer, D. C. Miller, and R. Dauskardt, "Adhesion between template materials and UV-cured nanoimprint resists," *Journal of Vacuum Science & Technology B: Microelectronics and Nanometer Structures,* vol. 25, p. 1179, 2007.

[40] B. Faircloth, H. Rohrs, R. Tiberio, R. Ruoff, and R. R. Krchnavek, "Bilayer, nanoimprint lithography," *Journal of Vacuum Science & Technology B: Microelectronics and Nanometer Structures,* vol. 18, p. 1866, 2000.

[41] R. W. Jaszewski, H. Schift, B. Schnyder, A. Schneuwly, and P. Groning, "The deposition of anti-adhesive ultra-thin teflon-like films and their interaction with polymers during hot embossing," *Applied Surface Science,* vol. 143, p. 301, 1999.

[42] I. Martini, S. Kuhn, M. Kamp, L. Worschech, A. Forchel, D. Eisert, *et al.*, "Fabrication of quantum point contacts by imprint lithography and transport studies," *Journal of Vacuum Science & Technology B: Microelectronics and Nanometer Structures,* vol. 18, p. 3561, 2000.

[43] P. Silberzan, L. Leger, D. Ausserre, and J. J. Benattar, "Silanation of silica surfaces. A new method of constructing pure or mixed monolayers," *Langmuir,* vol. 7, p. 1647, 1991.

[44] J. D. L. Grange and J. L. Markham, "Effects of surface hydration on the deposition of silane monolayers on silica," *Langmuir,* vol. 9, p. 1749, 1993.

[45] C. P. Tripp, R. P. N. Veregin, and M. L. Hair, "Effect of fluoroalkyl substituents on the reaction of alkylchlorosilanes with silica surfaces," *Langmuir,* vol. 9, p. 3518, 1993.

[46] T. Bailey, B. J. Choi, M. Colburn, M. Meissl, S. Shaya, J. G. Ekerdt, *et al.*, "Step and flash imprint lithography: Template surface treatment and defect analysis," *Journal of Vacuum Science & Technology B: Microelectronics and Nanometer Structures,* vol. 18, p. 3572, 2000.

[47] L. J. Guo, "Recent progress in nanoimprint technology and its applications," *Journal of Physics D: Applied Physics,* vol. 37, p. R123, 2004.

[48] M. B. Chan-Park, Y. Yan, W. K. Neo, W. Zhou, J. Zhang, and C. Y. Yue, "Fabrication of high aspect ratio poly(ethylene glycol)-containing microstructures by UV embossing," *Langmuir,* vol. 19, p. 4371, 2003.

[49] H. Lee and G.-Y. Jung, "Full wafer scale near zero residual nano-imprinting lithography using UV curable monomer solution," *Microelectronic Engineering,* vol. 77, p. 42, 2005.

[50] R. Yang, S. A. Soper, and W. Wang, "A new UV lithography photoresist based on composite of EPON resins 165 and 154 for fabrication of high-aspect-ratio microstructures," *Sensors and Actuators A: Physical,* vol. 135, p. 625, 2007.

[51] H. Lorenzyz, M. Despont, N. Fahrni, N. LaBianca, P. Renaud, and P. Vettiger, "SU-8: a low-cost negative resist for MEMS," *Journal of Micromechanics and Microengineering,* vol. 7, p. 121, 1997.

[52] Y. Morita, S. Tajima, H. Suzuki, and H. Sugino, "Thermally initiated cationic polymerization and properties of epoxy siloxane," *Journal of Applied Polymer Science,* vol. 100, p. 2010, 2006.

[53] X. Cheng, L. J. Guo, and P.-f. Hu, "Room-temperature, low-pressure nanoimprinting based on cationic photopolymerization of novel epoxysilicone monomers," *Advanced Materials,* vol. 17, p. 1419, 2005.

[54] D. Ye, P.-I. Wang, Z. Ye, Y. Ou, R. Ghoshal, R. Ghoshal, *et al.*, "UV nanoimprint lithography of sub-100nm nanostructures using a novel UV curable epoxy siloxane polymer," *Microelectronic Engineering,* vol. 87, p. 2411, 2010.

[55] P.-I. Wang, O. Nalamasu, R. Ghoshal, R. Ghoshal, C. D. Schaper, A. Li, *et al.*, "Novel photocurable epoxy siloxane polymers for photolithography and imprint lithography applications," *Journal of Vacuum Science & Technology B: Microelectronics and Nanometer Structures,* vol. 26, p. 244, 2008.

[56] A. S. P. Chang, K. J. Morton, H. Tan, P. F. Murphy, W. Wu, and S. Y. Chou, "Tunable liquid crystal-resonant grating filter fabricated by nanoimprint lithography," *IEEE Photonics Technology Letters,* vol. 19, p. 1457, 2007.

[57] F. Carcenac, C. Vieu, A. Lebib, Y. Chen, L. Manin-Ferlazzo, and H. Launois, "Fabrication of high density nanostructures gratings used as molds for nanoimprint lighography," *Microelectronic Engineering,* vol. 53, p. 163, 2000.

[58] S. Zankovych, T. Hoffmann, J. Seekamp, J.-U. Bruch, and C. M. S. Torres, "Nanoimprint lithography: challenges and prospects," *Nanotechnology,* vol. 12, p. 91, 2001.

[59] J. Kettle, S. Whitelegg, A. M. Song, D. C. Wedge, L. Kotacka, V. Kolarik, *et al.*, "Fabrication of planar organic nanotransistors using low temperature thermal nanoimprint lithography for chemical sensor applications," *Nanotechnology,* vol. 21, p. 075301, 2010.

[60] L. Guo, E. Leobandung, and S. Y. Chou, "A silicon single-electron transistor memory," *Science,* vol. 275, p. 649, 1997.

[61] Z. Yu, W. Wu, L. Chen, and S. Y. Chou, "Fabrication of large area 100 nm pitch grating by spatial frequency doubling and nanoimprint lithography for subwavelength optical applications," *Journal of Vacuum Science & Technology B: Microelectronics and Nanometer Structures,* vol. 19, p. 2816, 2001.

[62] C.-y. Chao and L. J. Guo, "Polymer microring resonators fabricated by nanoimprint technique," *Journal of Vacuum Science & Technology B: Microelectronics and Nanometer Structures,* vol. 20, p. 2862, 2002.

[63] I. Puscasu, G. Boreman, R. C. Tiberio, D. Spencer, and R. R. Krchnavek, "Comparison of infrared frequency selective surfaces fabricated by direct-write electron-beam and bilayer nanoimprint lithographies," *Journal of Vacuum Science & Technology B: Microelectronics and Nanometer Structures,* vol. 18, p. 3578, 2000.

[64] N. S. Ong, Y. H. Koh, and Y. Q. Fu, "Microlens array produced using hot embossing process," *Microelectronic Engineering,* vol. 60, p. 365, 2002.

[65] C. David, P. Ha ̈berling, M. Schnieper, J. So ̈chtig, and C. Zschokke, "Nano-structured anti-reflective surfaces replicated by hot embossing," *Microelectronic Engineering,* vol. 61-62, p. 435, 2002.

[66] Z. Yu, S. J. Schablitsky, and S. Y. Chou, "Nanoscale GaAs metal–semiconductor–metal photodetectors fabricated using nanoimprint lithography," *Applied Physics Letters,* vol. 74, p. 2381, 1999.

[67] E. Abad, S. Merino, A. Retolaza, and A. Juarros, "Design and fabrication using nanoimprint lithography of a nanofluidic device for DNA stretching applications," *Microelectronic Engineering,* vol. 85, p. 818, 2008.

[68] M. Beck, F. Persson, P. Carlberg, M. Graczyk, I. Maximov, T. G. I. Ling, *et al.*, "Nanoelectrochemical transducers for (bio-) chemical sensor applications fabricated by nanoimprint lithography," *Microelectronic Engineering,* vol. 73-74, p. 837, 2004.

[69] M. Bender, A. Fuchs, U. Plachetka, and H. Kurz, "Status and prospects of UV-Nanoimprint technology," *Microelectronic Engineering,* vol. 83, p. 827, 2006.

[70] S. Park, Z. Song, L. Brumfield, A. Amirsadeghi, and J. Lee, "Demolding temperature in thermal nanoimprint lithography," *Applied Physics A,* vol. 97, p. 395, 2009.

[71] X. Wang, Y. Chen, S. Banu, H. Morgan, S. Fu, and Z. Cui, "High density patterns fabricated in SU-8 by UV curing nanoimprint," *Microelectronic Engineering,* vol. 84, p. 872, 2007.

[72] M. D. Austin, H. Ge, W. Wu, M. Li, Z. Yu, D. Wasserman, *et al.*, "Fabrication of 5 nm linewidth and 14 nm pitch features by nanoimprint lithography," *Applied Physics Letters,* vol. 84, p. 5299, 2004.

[73] R. L. Jones, T. Hu, C. L. Soles, E. K. Lin, R. M. Reano, S. W. Pang, *et al.*, "Real-time shape evolution of nanoimprinted polymer structures during thermal annealing," *Nano Letters,* vol. 6, p. 1723, 2006.

[74] Y. Ding, H. W. Ro, J. F. Douglas, R. L. Jones, D. R. Hine, A. Karim, *et al.*, "Polymer viscoelasticity and residual stress effects on nanoimprint lithography," *Advanced Materials,* vol. 19, p. 1377, 2007.

[75] T. Leveder, E. Rognin, S. Landis, and L. Davoust, "Reflow of supported sub-100nm polymer films as a characterization process for NanoImprint lithography," *Microelectronic Engineering,* vol. 88, p. 1867, 2011.

[76] P. E. Rouse Jr, "A theory of the linear viscoelastic properties of dilute solutions of coiling polymers," *The Journal of Chemical Physics,* vol. 21, p. 1272, 1953.

[77] H. Watanabe, "Viscoelasticity and dynamics of entangled polymers," *Progress in Polymer Science,* vol. 24, pp. 1253-1403, 1999.

[78] K. Kremer and G. S. Grest, "Dynamics of entangled linear polymer melts: A molecular‐dynamics simulation," *The Journal of Chemical Physics,* vol. 92, pp. 5057-5086, 1990.

[79] R. H. Colby, L. J. Fetters, and W. W. Graessley, "The melt viscosity-molecular weight relationship for linear polymers," *Macromolecules,* vol. 20, pp. 2226-2237, 1987.

[80] L. Fetters, D. Lohse, D. Richter, T. Witten, and A. Zirkel, "Connection between polymer molecular weight, density, chain dimensions, and melt viscoelastic properties," *Macromolecules,* vol. 27, pp. 4639-4647, 1994.

[81] S. Wu, "Predicting chain conformation and entanglement of polymers from chemical structure," *Polymer Engineering & Science,* vol. 32, pp. 823-830, 1992.

[82] K.-i. Akabori, K. Tanaka, T. Nagamura, A. Takahara, and T. Kajiyama, "Molecular motion in ultrathin polystyrene films dynamic mechanical analysis of surface and interfacial effects," *Macromolecules,* vol. 38, p. 9735, 2005.

[83] W. Gawrisch, M. G. Brereton, and E. W. Fischer, "A new method for data evaluation of small angle neutron scattering experiments and its application to amorphous polycarbonate," *Polymer Bulletin,* vol. 4, p. 687, 1981.

[84] H. Yoon, H. S. Cho, K. Y. Suh, and K. Char, "Step-and-repeat process for thermal nanoimprint lithography," *Nanotechnology,* vol. 21, p. 105302, Mar 12 2010.

[85] K.-i. Nakamatsu, K. Watanabe, K. Tone, T. Katase, W. Hattori, Y. Ochiai, *et al.*, "Bilayer resist method for room-temperature nanoimprint lithography," *Japanese Journal of Applied Physics,* vol. 43, p. 4050, 2004.

[86] R. Suzuki, N. Sakai, A. Sekiguchi, Y. Matsumoto, R. Tanaka, and Y. Hirai, "Evaluation of curing characteristics in UV-NIL resist," *Journal of Photopolymer Science and Technology,* vol. 23, p. 51, 2010.

[87] Z. Yu, P. Deshpande, W. Wu, J. Wang, and S. Y. Chou, "Reflective polarizer based on a stacked double-layer subwavelength metal grating structure fabricated using nanoimprint lithography," *Applied Physics Letters,* vol. 77, p. 927, 2000.

[88] N. An, Y. Li, Y. Yang, F. Yu, and L. Dong, "Stabilization of polymer bilayers by introducing crosslinking at the interface," *Macromolecular Rapid Communications,* vol. 27, p. 955, 2006.

[89] E. M. Woo and M. N. Wu, "Blends of a diglycidylether epoxy with bisphenol-A polycarbonate or poly(methyl methacrylate)," *Polymer,* vol. 37, p. 2845, 1996.

[90] E. M. Woo, "Reaction-induced phase separation in a semiinterpenetrating network of reactive ternary blends," *Journal of Polymer Science Part A: Polymer Chemistry,* vol. 34, p. 781, 1996.

[91] B. H. Stuart and P. S. Thomas, "Xylene swelling of polycarbonate studied using Fourier transform Raman spectroscopy," *Spectrochimica Acta Part A,* vol. 51, p. 2133, 1995.

[92] A. Kulczycki, "Calculation of the vibrational frequencies of crystalline bispbeool A polycarbonate," *Spcfrochimica Acra,* vol. 41A, p. 1427, 1985.

[93] P. Schmidt and J. Dybal, "Conforrnational structure of bisphenol A polycarbonate studied by infra-red spectroscopy," *Polymer,* vol. 32, p. 1862, 1991.

[94] T. Higashiki, T. Nakasugi, and I. Yoneda, "Nanoimprint lithography for semiconductor devices and future patterning innovation," *SPIE Proceedings,* vol. 7970, p. 797003, 2011.

[95] M. Malloy, L. C. Litt, S. Johnson, D. J. Resnick, and D. Lovell, "Jet and flash imprint defectivity: assessment and reduction for semiconductor applications," *SPIE Proceedings*, vol. 7970, p. 797006, 2011.

[96] M. Colburn, I. Suez, B. J. Choi, M. Meissl, T. Bailey, S. V. Sreenivasan, *et al.*, "Characterization and modeling of volumetric and mechanical properties for step and flash imprint lithography photopolymers," *Journal of Vacuum Science & Technology B: Microelectronics and Nanometer Structures*, vol. 19, p. 2685, 2001.

[97] M. Shibata, A. Horiba, Y. Nagaoka, H. Kawata, M. Yasuda, and Y. Hirai, "Process-simulation system for UV-nanoimprint lithography," *Journal of Vacuum Science & Technology B: Microelectronics and Nanometer Structures*, vol. 28, p. C6M108, 2010.

[98] S. Johnson, R. Burns, E. K. Kim, M. Dickey, G. Schmid, J. Meiring, *et al.*, "Effects of etch barrier densification on step and flash imprint lithography," *Journal of Vacuum Science & Technology B: Microelectronics and Nanometer Structures*, vol. 23, p. 2553, 2005.

[99] Q. Wang, H. Hiroshima, and H. Atobe, "A dynamic system to evaluate the UV shrinkage characteristics of UV photopolymers used for nanoimprint," *Journal of Photopolymer Science and Technology*, vol. 23, pp. 33-38, 2010.

[100] A. Horiba, M. Yasuda, H. Kawata, M. Okada, S. Matsui, and Y. Hirai, "Impact of resist shrinkage and its correction in nanoimprint lithography," *Japanese Journal of Applied Physics*, vol. 51, p. 06FJ06, 2012.

[101] A. Amirsadeghi, J. J. Lee, and S. Park, "Polymerization shrinkage stress measurement for a UV-curable resist in nanoimprint lithography," *Journal of Micromechanics and Microengineering,* vol. 21, p. 115013, 2011.

[102] M. Vogler, S. Wiedenberg, M. Mühlberger, I. Bergmair, T. Glinsner, H. Schmidt, *et al.*, "Development of a novel, low-viscosity UV-curable polymer system for UV-nanoimprint lithography," *Microelectronic Engineering,* vol. 84, p. 984, 2007.

[103] P. Voisin, M. Zelsmann, R. Cluzel, E. Pargon, C. Gourgon, and J. Boussey, "Characterisation of ultraviolet nanoimprint dedicated resists," *Microelectronic Engineering,* vol. 84, p. 967, 2007.

[104] V. Geiser, Y.-H. Jin, Y. Leterrier, and J.-A. E. Månson, "Nanoimprint lithography with UV-curable hyperbranched polymer nanocomposites," *Macromolecular Symposia,* vol. 296, p. 144, 2010.

[105] D. T. Vodak, M. Braun, L. Iordanidis, J. Plevert, M. Stevens, L. Beck, *et al.*, "One-step synthesis and structure of an oligospiroorthocarbonate," *Journal of American Chemistry Society,* vol. 124, p. 4942, 2002.

[106] G. Rokicki, "Aliphatic cyclic carbonates and spiroorthocarbonates as monomers," *Progress in Polymer Science,* vol. 25, p. 259, 2000.

[107] F. Sanda and T. Endo, "Radical ring-opening polymerization," *Journal of Polymer Science Part A: Polymer Chemistry,* vol. 39, p. 265, 2001.

[108] T. Hino and T. Endo, "A novel synthetic approach to networked polymers without volume shrinkage on cross-linking polymerization: cationic

copolymerization of a monofunctional epoxide and a spiro orthocarbonate bearing norbornene backbone," *Macromolecules,* vol. 36, p. 5902, 2003.

[109] M. Sangermano, R. A. Ortiz, B. A. P. Urbina, L. B. Duarte, A. E. G. Valdez, and R. G. Santos, "Synthesis of an epoxy functionalized spiroorthocarbonate used as low shrinkage additive in cationic UV curing of an epoxy resin," *European Polymer Journal,* vol. 44, p. 1046, 2008.

[110] T. Takata, T. Ariga, and T. Endo, "Cationic ring-opening polymerizations of five-membered spiro orthocarbonates: Unsubstituted and 2,8-Diaryl-1,4,6,9-tetraoxaspiro[4.4]nonanes," *Macromolecules,* vol. 25, p. 3829, 1992.

[111] T. Nishino, M. Meguro, K. Nakamae, M. Matsushita, and Y. Ueda, "The lowest surface free energy based on -CF3 alignment," *Langmuir,* vol. 15, p. 4321, 1999.

[112] T. Hino and T. Endo, "Lewis acid-mediated double ring-opening reaction of an oligo(spiro-orthocarbonate): A novel class of expanding material," *Journal of Polymer Science Part A: Polymer Chemistry,* vol. 43, p. 5323, 2005.